An FMI-based co-simulation framework for simulations of wave energy converter systems

Energy Conversion and Management 323 (2025) 119220

Contents lists available at ScienceDirect

Energy Conversion and Management

journal homepage: www.elsevier.com/locate/enconman

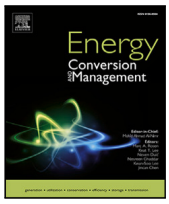

An FMI-based co-simulation framework for simulations of wave energy converter systems

Xinyuan Shao [a,*], Jonas W. Ringsberg [a], Erland Johnson [a,b], Zhiyuan Li [a], Hua-Dong Yao [a], Jan G. Skjoldhammer [c], Stefan Björklund [c]

[a] Chalmers University of Technology, Department of Mechanics and Maritime Sciences, Division of Marine Technology, SE-41296 Gothenburg, Sweden
[b] RISE Research Institutes of Sweden, Department of Applied Mechanics, SE-50462 Borås, Sweden
[c] Novige AB, SE-18730 Stockholm, Sweden

ARTICLE INFO

Keywords:
FMI-based co-simulation
Global system modelling
Interaction effects
Power performance
Wave energy converter
Wave park

ABSTRACT

A wave energy converter (WEC) comprises many components with distinct functions. The whole WEC system is complicated, as each component is also a complex subsystem. It is challenging to properly model and couple these subsystems to achieve a global simulation of the whole system. This study proposes an FMI-based co-simulation framework to tackle this challenge. Through the use of a co-simulation technique requiring minimal programming effort, a suite of numerical solvers serving for modelling various WEC components is coupled to create a comprehensive system model for a single WEC unit. The modules of the Ansys software, Aqwa and Rigid Dynamics, are employed to model hydrodynamic loads and motion responses. Simulink is utilized to model the power take-off (PTO) system and then integrate all models into a global simulation. The capability and accuracy of the FMI-based co-simulation framework are validated against an experimental heave decay test and verified by cross-comparing a numerical model built in SESAM. Furthermore, the framework is expanded to encompass the modelling of a large-scale wave park that includes multiple WEC units. Based on a novel WEC concept called NoviOcean, two study cases of a single unit and an 18-unit wave park are investigated. Buoy motions and power performance under several regular and irregular sea states are analysed. The hydrodynamic interactions between the units are evaluated quantitatively regarding the power performance. It is found that the interactions improve the power performance, with a maximum increase of up to 36%.

1. Introduction

Wave energy, as a promising renewable energy source, has gained attention in the global energy market due to its large power density and round-the-clock availability compared to solar and wind energy [1–3]. Various types of wave energy converters (WECs) were invented by research communities and companies, such as oscillating water columns, oscillating bodies, and overtopping devices [4]. Although some of them have shown technical feasibility, none has been fully commercialized. Systematic numerical simulation tools must be found to enable fast design iterations for WECs at the early development stage to speed up the full commercialization process.

WECs are complex systems with many multidisciplinary subsystems, for example, the hydrodynamic system, including buoys and floaters; the mechanical system, including shafts and gearbox; the power take-off (PTO) system; and the mooring system. These systems couple with each other and have a joint influence on the overall performance of the WECs installed in a wave park. This brings about an obvious challenge that the design of WECs is a mixture of endeavours from different research teams and companies since the development of each subsystem requires specific methods and tools. However, the available commercial software, such as Ansys Aqwa [5], SESAM [6] and OrcaFlex [7], were initially designed for ship and offshore platform hydrodynamic and structural simulations, so they are inherently not good at dealing with multi-system and multidisciplinary simulations. That is why in many existing numerical studies, either the type of WEC is restricted to single-body devices, or multi-body devices but with limited types of joint connections that software allows, or some simplifications have to be made. For example, Yang et al. [8,9] studied a floating point absorber WEC using numerical simulation in SESAM and the results showed good agreement with experiments. However, their numerical model was a single-body WEC with a simplified PTO system as a linear damper and their study focused more on the hydrodynamic and mooring system instead of considering the WEC system as a whole. Their approach is commonly used to model floating point absorber

* Corresponding author.
E-mail address: xinyuan.shao@chalmers.se (X. Shao).

https://doi.org/10.1016/j.enconman.2024.119220
Received 25 June 2024; Received in revised form 27 September 2024; Accepted 1 November 2024
Available online 14 November 2024

WECs with relatively simple mechanical systems. Similar studies can also be found in [10,11].

However, the mechanical system of WECs is becoming more complicated. SJTU-WEC in [12] has a 4-bar linkage, a spherical linkage and a bevel gear to transform WEC motions into rotations to the hydraulic motors. A raft-type WEC in [13] has hinges and torsion bistable mechanisms between each raft to enhance its power absorption efficiency. A dual turbine wheel WEC proposed in [14] uses a belt-drive mechanical transmission system to amplify the rotational speed of the generator. A hybrid wave–current energy converter in [15] includes a gearbox containing bearings, bevel gears, clutches, cases and shafts to collect inputs from waves and current to produce output to the generator. Other WEC examples with complex mechanical systems can be found in [16–21]. Complex mechanical systems are also common in combined WEC-wind energy converters as in [22–26].

New methods must be found for WECs with complex mechanical systems or multiple WECs with explicit mechanical connections to capture their characteristics better. One example of the latter can be found in [27], where multiple WECs are connected by spherical joints and linking arms to form a hex WEC-net. They analysed such a complicated interconnected system by coupling a computational fluid dynamic (CFD) solver with a multi-body dynamic (MBD) solver. The two solvers computed the hydrodynamic forces and the resulting motions, respectively. Communication between the two solvers was achieved with the help of TCP/IP protocol at each iteration in each step. The results indicated that the motion of the whole system is strongly affected by the mechanical system.

The design and control of the PTO system is a hot topic to increase the power efficient and reduce the WEC's capital cost of energy. To have a general impression of the techniques used in PTO systems, the readers can refer to some review articles as [28–30]. For most PTO systems, for example, hydraulic PTO systems in [31–33], their behaviours are nonlinear and, therefore, cannot be modelled by simplified linear damper models. The PTO system needs to be modelled in detail and coupled with other subsystems to consider its overall effects on the global system, which is necessary for the development of effective control laws to enhance power efficiency. Moreover, the hydrodynamic and mooring systems of WECs have been studied intensively. Some research focuses are WEC hydrodynamic performance [34–36], mooring fatigue damage [9,36] and interaction effects within wave parks [37–39].

To better capture the characteristics of a WEC system, it is useful to find an efficient way to include all detailed subsystem models, namely, hydrodynamic, mechanical, PTO and mooring systems, into a global model and have a more accurate global simulation. The dilemma is that not a single software nowadays can fulfil the requirement completely.

Coupling different software or tools is a strategy commonly used to overcome the limitations of a single software and include all subsystem models into one global model. Many examples can be found in recent research, and they are not restricted to the wave energy field but also the floating offshore wind area. Palm et al. [40] coupled MooDy, an in-house mooring code, with OpenFOAM, a CFD solver, to achieve a fully coupled CFD-mooring analysis. Penalba et al. [41] coupled OpenFOAM with Matlab where the PTO model was developed. Similar to WEC systems, floating offshore wind turbines also contain many subsystems. Therefore, the coupling strategy is also popular in their field. Yang et al. [42], Cao et al. [43], Han et al. [44] and Jin et al. [45] used a dynamically linked library (DLL) to couple Ansys Aqwa with OpenFAST to analyse either a floating offshore wind turbine or a hybrid system with wind turbine and WECs. Although the above-mentioned ways are proper candidates to couple the subsystems of WECs, the problem is that they all need in-house programs to handle the communication between solvers. Moreover, the communication program is highly unlikely to be universal, meaning that the program probably needs to be rewritten when the computational environment or solver changes.

To overcome the above-mentioned limitations when coupling different tools, a co-simulation strategy based on the functional mock-up interface (FMI) is an effective way. Mono-disciplinary models can be developed separately and then coupled using the standardized interfaces FMI [46] to enable subsystem communication within the same platform. Each subsystem is encapsulated as a functional mock-up unit (FMU), a black box that can consume inputs, carry out calculations and provide outputs. By properly connecting the corresponding inputs and outputs of different FMUs in FMI-supporting platforms like Ansys Twin Builder [47] and Simulink [48], the subsystems can cooperate in an organic way to do comprehensive global simulations without writing explicit programs for data communication between different solvers. The FMI-based co-simulation has been broadly applied to many fields, for example, hybrid vehicles [49], maritime cranes [50], and hydraulic excavators [51]. It successfully coupled multiple solvers and tools to form global simulations and gave satisfactory results. Even though the FMI-based co-simulation has not been adopted widely in the wave energy field, its simplicity and standardization make it also promising for academic research and industrial developments of WECs.

Compared with current state-of-art WEC system simulation, the co-simulation has three main advantages. Firstly, the co-simulation can couple different software and tools to model the behaviours of different subsystems without simplifying complex subsystems due to the limitations of a single software. Secondly, unlike using DLL to couple different solvers, the co-simulation does not require explicit programming effort. The data synchronization between different solvers is handled by the co-simulation algorithm provided by some FMI-supporting platforms. This enables engineers to focus on pure engineering questions. Thirdly, under the co-simulation framework, the modelling and development of each subsystem can be distributed to teams with different expertise as long as they encapsulate their model into FMUs at the end. The global model can be easily built by combining the FMUs in FMI-supporting platforms. This feature enables multidisciplinary corporations between different engineering teams.

This study aims to establish a modularized and portable FMI-based co-simulation framework for WECs with complex mechanical systems that can hardly be modelled using a single software. The methodology will be firstly validated by an experimental benchmark study and then verified by a code-to-code comparison with SESAM. The methodology will be applied to model NoviOcean, a kind of WEC consisting of a pontoon-shaped buoy, a seabed-fixed piston rod, a water tube and a Pelton turbine. The hydrodynamic-mooring, mechanical, and PTO systems are modelled in separate modules using different tools. The global simulation is conducted in the Simulink environment. To further verify the reliability of this method, a wave park with 18 WECs is simulated. To the authors' knowledge, it is the first time that FMI-based co-simulation applies to wave park simulations. The dynamic response and power performance of the wave park are quantitatively evaluated.

2. Methodology

This section describes the modelling of each subsystem of a general WEC and how they are coupled within the co-simulation framework.

2.1. Co-simulation framework under the FMI standard

FMI is a tool-independent and free-to-use standard first developed in the project Modelisar from 2008 to 2011 [52]. The FMI standard defines the interface between a model and a simulation environment. FMI supports co-simulations which use multiple FMUs containing both the model information and the corresponding solver to build a global model. The structure of a general co-simulation is shown in Fig. 1. It is worth noting that the co-simulation algorithm is not a part of the FMI standard. It is instead provided by importing tools, such as Simulink which is adopted in this study. The main task of a co-simulation algorithm is to advance the overall simulation time and exchange data between multiple FMUs, while the FMI standard only defines the interface of a single FMU [53].

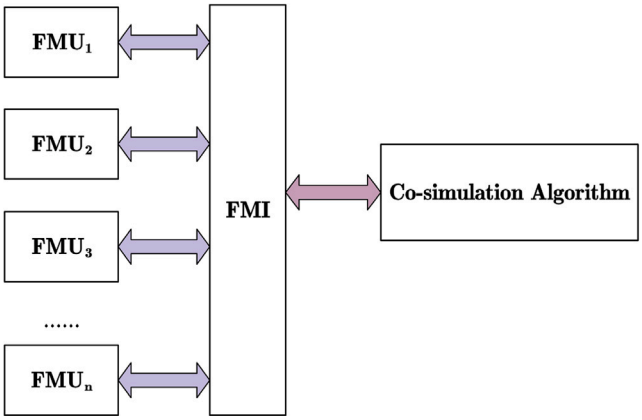

Fig. 1. Diagram of a general FMI-based co-simulation model.

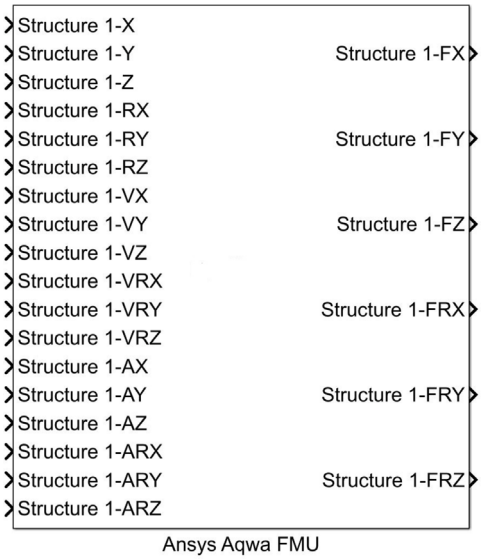

Fig. 2. An example of an FMU exported by Ansys Aqwa.

FMI is a well-accepted standard of many commercial software, for example, Ansys Aqwa and Ansys Rigid Dynamics. In FMUs exported by software following the FMI standard, the numerical models built in different tools are encapsulated as black boxes with standardized input and output pins. Fig. 2 shows an example of an FMU exported by Ansys Aqwa with structure motions (positions/displacements, velocities, and accelerations) as the inputs and resulting total forces (forces and moments) as the outputs in different coordinate directions. A global model can be achieved by properly connecting the inputs and outputs of different FMUs.

The FMI-based co-simulation framework mitigates the knowledge gap between the producers and users of FMUs. It is useful for developing complex system models by decoupling the modelling process of each subsystem within different disciplines. Also, it removes the barriers between specialized engineers and programmers, as establishing a co-simulation model does not require explicit programming effort. These advantages make it highly promising in a broad collection of industrial applications.

2.2. Hydrodynamic-mooring system model

The hydrodynamic system in this study refers to the buoy of a floating point absorber. The linear potential theory is used to solve the hydrodynamic and hydrostatic forces. The fundamental equation of the linear potential theory is the Laplace equation. The theoretical derivation of the Laplace equation, the boundary conditions, the solving method and the calculation of hydrodynamic pressure forces based on the velocity potential can be found in Chapter 4 of Newman's textbook [54]. The linearizations taken in the linear potential theory are twofold, including the linearization of the free-surface boundary conditions and the assumption that the velocity potential can be divided into independent parts, namely, the incident, diffracted and radiated potentials. Detailed description and derivation of the linearization can be found in Chapter 6.1 of Newman's textbook [54] and Chapters 2 and 3 of Faltinsen's textbook [55].

Ansys Aqwa can solve the Laplace equation under the assumptions of the linear potential theory using the boundary element method (BEM) in the frequency domain, and then compute the hydrodynamic coefficients and impulse response function for radiation force calculation in the time domain. The wave excitation force is computed by the wave excitation transfer function.

Ansys Aqwa is also capable of modelling the mooring system. In this study, the mooring line is modelled using the dynamic composite catenary mooring line theory, which considers the effects of the mooring line mass, drag forces and inline tensions in a fully coupled way. It means that the mooring forces and the body's motion affect each other mutually. The nonlinear axial stiffness of the mooring line is defined as:

$$EA = EA_{\text{unstrained}} + k_1\varepsilon + k_2\varepsilon^2. \tag{1}$$

where $EA_{\text{unstrained}}$ is the unstrained axial stiffness, k_1 and k_2 are first-order and second-order axial stiffness coefficients, and ε is the strain of the mooring line. Readers can refer to Chapters 9.7 and 13 of Ansys Aqwa theory manual [56] for further details about the theory used in mooring analyses and time domain dynamic simulations.

The FMU exported by Ansys Aqwa can compute the total force and moment of hydrostatic, hydrodynamic (excitation and radiation) and mooring loads based on the instantaneous motions of the body. The FMU's inputs are the motions of the body, while the outputs are the total forces and moments written as:

$$\mathbf{F}_{AqwaFMU} = \mathbf{F}_{hydrostatic} + \mathbf{F}_{excitation} + \mathbf{F}_{radiation} + \mathbf{F}_{mooring}. \tag{2}$$

Note that $\mathbf{F}_{radiation}$ excludes the added mass component of the radiation force, $\mathbf{A}\big|_{\omega=\infty}\ddot{\mathbf{X}}$, as it is computed in the mechanical system model which is introduced in Section 2.3. The loads due to wind and ocean currents are not included in this study.

2.3. Mechanical system model

The mechanical system refers to components that convert input motions and forces into desired output motions and forces. For a WEC system, the mechanical system can be shafts, joints and mechanical components within the PTO system like a gearbox. The mechanical system restricts the motion of a WEC under the wave load and, therefore, has some influences on the power performance. Ansys Aqwa can simulate the connections between structural components using joints. However, the types of joints are restricted to ball, universal, hinge and locked joints, which cannot properly capture the characteristics of complex mechanical systems.

Ansys Rigid Dynamics can be used to build models of rigid bodies connected by joints and springs. The available types of connections are more than those in Ansys Aqwa. Ansys Rigid Dynamics solves the equation of motion:

$$\left(\mathbf{M} + \mathbf{A}\big|_{\omega=\infty}\right)\ddot{\mathbf{X}} + \mathbf{C}\dot{\mathbf{X}} + \mathbf{K}\mathbf{X} = \mathbf{F}_{AqwaFMU} + \mathbf{F}_{PTO}, \tag{3}$$

where $\mathbf{M}$ is the mass matrix, $\mathbf{A}\big|_{\omega=\infty}$ is the added mass matrix at the infinite frequency, $\mathbf{C}$ is the damping matrix caused by components within the mechanical system, $\mathbf{K}$ is the stiffness matrix and $\mathbf{F}_{PTO}$ is the

force introduced by the PTO system which is presented in Section 2.4. For the FMU exported by Ansys Rigid Dynamics, $\mathbf{F}_{AqwaFMU}$ and $\mathbf{F}_{PTO}$ are its inputs, while the position, velocity and acceleration are its outputs.

2.4. PTO system model

The conversion of wave energy into electricity is a manifold process. As summarized in [57], the whole process consists of three energy conversion stages. The primary energy conversion for floating point absorber WECs transforms wave energy into mechanical energy. That is, the hydrodynamic body of a WEC is driven by waves to move. In the secondary conversion stage, the mechanical energy of the WEC is converted into useful mechanical energy by a specific PTO system which is usually hydraulic for point absorbers. The final stage is a further conversion from mechanical energy into electricity by the generators within the PTO system. This study considers only the first energy conversion stage, from wave energy to mechanical energy. Integrating the latter two stages into the global simulation is possible when the models of hydraulic cylinders and generators are available.

Including the mechanical components of a PTO system, such as pistons and shafts, in the mechanical system model is convenient since a rigid dynamic solver can also solve their motions. On the other hand, the uniqueness of the PTO system is the damping effect and the possible control strategy, which can be considered separately in a PTO system model. It is worth noting that the development of possible control strategies is beyond the scope of this paper, but the methodology proposed in this study provides a straightforward interface for such development together with other subsystems by using the inputs and outputs of FMUs. One example of integrating a PTO control strategy into a WEC co-simulation system can be found in [36]. In the present study, the PTO system is instead simplified as a linear damper with a damping coefficient of B_{PTO} for simplicity without reducing the clarity of the demonstration of the co-simulation framework. The reaction force generated by the PTO system is assumed to only act in the global vertical direction, which can be written as:

$$F_{PTO,z} = -B_{PTO}V_z, \tag{4}$$

where V_z is the velocity of the buoy in the vertical direction. The averaged hydrodynamic power captured by the PTO system is calculated as:

$$P = \frac{1}{T}\int_0^t B_{PTO}{V_z}^2 dt. \tag{5}$$

2.5. Hydrodynamic interaction

Hydrodynamic interaction refers to the radiation and diffraction effects caused by multiple bodies. It concerns the influence of one body's flow field on another's. As the hydrodynamic interaction can alter the flow field, resulting in the change of hydrodynamic forces on each body, it is important to include the hydrodynamic interaction in wave park simulations.

Similar to single-body cases, the velocity potential of multi-body cases is solved by BEM considering the boundary conditions of each body. Compared with single-body cases, the dimension of the hydrodynamic coefficient matrix of multi-body cases is extended to $6\times M$ where M is the number of bodies. The wave excitation forces calculated by the solved diffracted velocity potential naturally integrates the diffraction effects caused by the hydrodynamic interaction. Readers can refer to Chapter 4.2.1 of Ansys Aqwa theory manual [56] for further details and formulas.

2.6. Co-simulation model of a WEC system and its limitations

Fig. 3 shows the diagram of a WEC system co-simulation model. Note that the WEC system is not restricted to a single WEC unit but can also be a wave park containing multiple WEC units. FMU_1 and FMU_2 are exported from Ansys Aqwa and Ansys Rigid Dynamics, respectively. The model of the simplified PTO system is directly modelled in Simulink. The co-simulation is also carried out in the Simulink environment.

The co-simulation model naturally inherits limitations of its subsystem models. The main limitations of the co-simulation model built for WECs in this study come from the limitation of Ansys Aqwa. Firstly, Ansys Aqwa assumes that the flow is inviscid and irrotational, meaning viscous effects are not inherently accounted for. The viscous effects can be added using damping factors from experiments or high-fidelity computational fluid dynamics (CFD) simulation. Secondly, the linear potential theory adopted by Ansys Aqwa assumes that waves and responses can be superimposed linearly, which is not the case for extreme sea states.

3. Validation and verification

Experimental data and code-to-code comparisons validate and verify the co-simulation methodology in this chapter.

3.1. Experimental heave decay test

In 2021, a series of highly accurate and precise heave decay tests were conducted on a sphere with a diameter D of 300 mm in the Ocean and Coastal Engineering Laboratory at Aalborg University, Denmark [58]. The physical test aimed to provide a high-quality benchmark dataset to validate and calibrate numerical models. A floating sphere was chosen as the experimental object. The sphere was dropped from three heights, $0.1D$, $0.3D$ and $0.5D$, corresponding to linear, moderately nonlinear, and highly nonlinear cases. Details of the physical model of the sphere, experimental settings and data collection equipment can be found in Section 1 and 2 of [58].

These tests provided rigorous benchmark datasets for numerical model validation with low uncertainties. We set a co-simulation model for the dropping sphere using the same parameters provided in [58]. Fig. 4 shows the co-simulation model of the free-dropping sphere. The inputs of the hydrodynamic system FMU are the positions, velocities and accelerations of the sphere with 6 degrees-of-freedom, while the outputs are the total forces and moments acting on the sphere. For the mechanical system FMU, its inputs and outputs are opposite to the hydrodynamic system FMU. The corresponding inputs and outputs are connected with arrows in the Simulink environment. Unlike a complete WEC system, the dropping sphere has neither a PTO nor a mooring system. The time step of the co-simulation is 0.001 s, the same as the time step of each subsystem. Note that there are memory blocks between the mechanical system FMU outputs and the hydrodynamic system FMU inputs to avoid algebraic loops which may happen when the inputs and outputs of the two FMUs are circularly dependent on each other at the same time step. The function of the memory blocks is to hold the outputs from the mechanical system FMU for one simulation time step and to provide inputs to the hydrodynamic system FMU using the most recent value from the last simulation step. Therefore, the circular dependency between the two FMUs can be broken by introducing the memory blocks.

Fig. 5 compares the results from co-simulations and the benchmark dataset from [58]. To better compare the data, the heave decay time series are normalized with the drop heights while the time is normalized by dividing the damped natural period in heave, which is 0.76 s as indicated in [58]. Besides the experimental data, the benchmark dataset provided in [58] also includes results from the numerical modelling blind test using various types of numerical models.

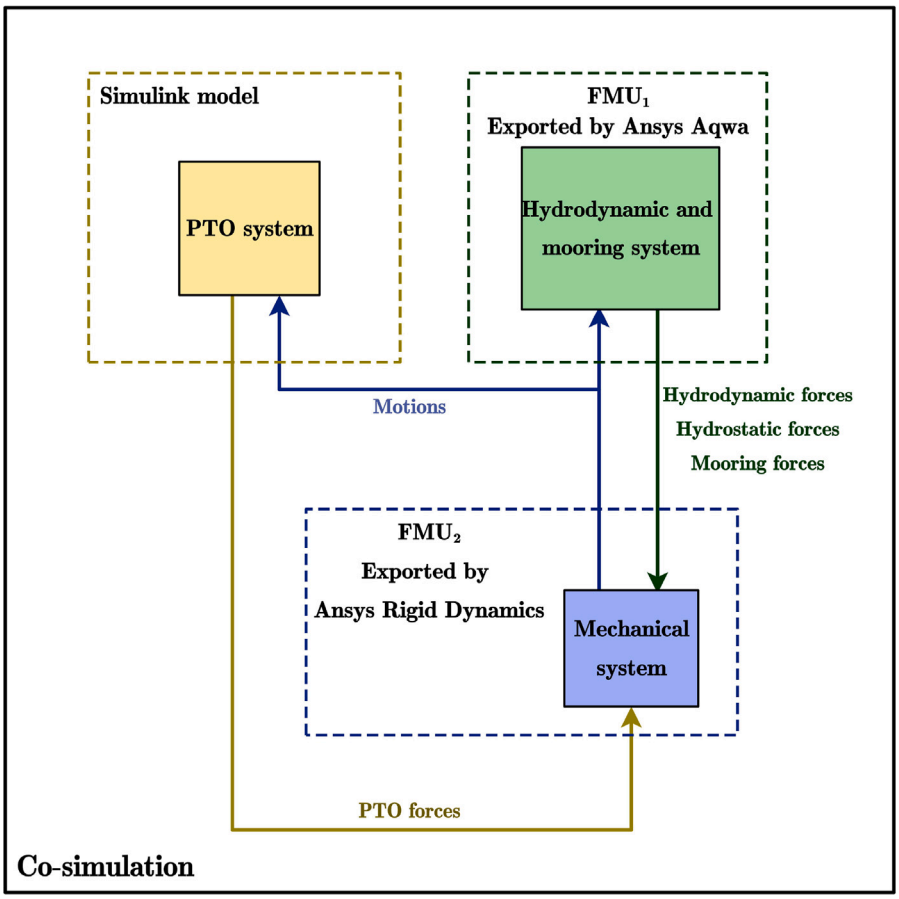

Fig. 3. Diagram of WEC system co-simulations.

The linear potential flow model 2 (LPF2) is one of them and it uses the nonlinear hydrostatics and linear radiation coefficients from the BEM code WAMIT [58].

Fig. 6 shows the quantitative differences between the three normalized decay time series shown in Fig. 5 by calculating the root mean square errors (RMSEs) between each pairs of the three time series. Regarding the RMSEs between the experimental and co-simulation results, it is observed that the nonlinear case with a dropping height of $0.5D$ is the one with the highest RMSE among all three cases. However, even so, the value of 0.063 is relatively small compared with the initial normalized dropping height of 1. The RMSEs between the LPF2 and the co-simulation results are less or equal to 0.015 for all three cases, indicating good agreement. The is because that the LPF2 adopts the same level of nonlinearity and uses the same theory as the hydrodynamic model of the co-simulation. Moreover, Table 1 listed the Pearson correlation coefficients ρ between the time series. The closer ρ is to 1, the higher the degree of linear correlation between the two time series. For all cases, each pair of the three time series has a correlation coefficient larger than 0.98, showing high linear correlation.

Considering the RMSEs and correlation coefficients, it is safe to conclude that the co-simulation results agree well with the experimental and LPF2 results, which indicates the capability of each FMU to carry out its own subsystem simulation and the co-simulation algorithm provided by Simulink to handle multi-solver communications.

3.2. Code-to-code verification

Even though the benchmark case in Section 3.1 has revealed the capability of co-simulation, the case of a dropping sphere does not include a mooring system and a PTO system, which are indispensable for a WEC system. Therefore, another complete WEC system test case is chosen to verify further the co-simulation methodology with the commercial software SESAM.

Table 1
Correlation coefficients. ρ_1 is the correlation coefficient between the experimental results and the co-simulation results. ρ_2 is the correlation coefficient between the experimental results and the LPF2 results. ρ_3 is the correlation coefficient between the LPF2 results and co-simulation results.

	ρ_1	ρ_2	ρ_3
$0.1D$	0.9981	0.9996	0.9996
$0.3D$	0.9981	0.9995	0.9993
$0.5D$	0.9895	0.9993	0.9899

WaveEL 4.0 is a floating point absorber developed by the company Waves4Power based on their former WaveEL 3.0. The main difference between the two versions is the length of its water tube. In [59], WaveEL 3.0 was modelled in SESAM, and the results show good agreement with experimental data, which validates the SESAM model. WaveEL 4.0, in this study, is modelled using the same procedures. The WaveEL 4.0 WEC system with the WEC and its 2-segment mooring system with one submerged floater in each mooring line are shown in Fig. 7. The main properties of the WEC system are listed in Table 2. Details about the geometrical dimension and basic properties of WaveEL 4.0 can be found in [59]. Fig. 25 in the Appendix shows the co-simulation model for WaveEL 4.0. The PTO system is modelled as a stand-alone module, which takes the vertical velocity of the WEC as the input and the damping force as the output. The PTO linear damping value was chosen as the same value as in the SESAM model. To better verify the co-simulation methodology, the co-simulation model and the SESAM model keep all other factors the same besides the PTO damping. The test case runs under a regular sea state with a wave amplitude of

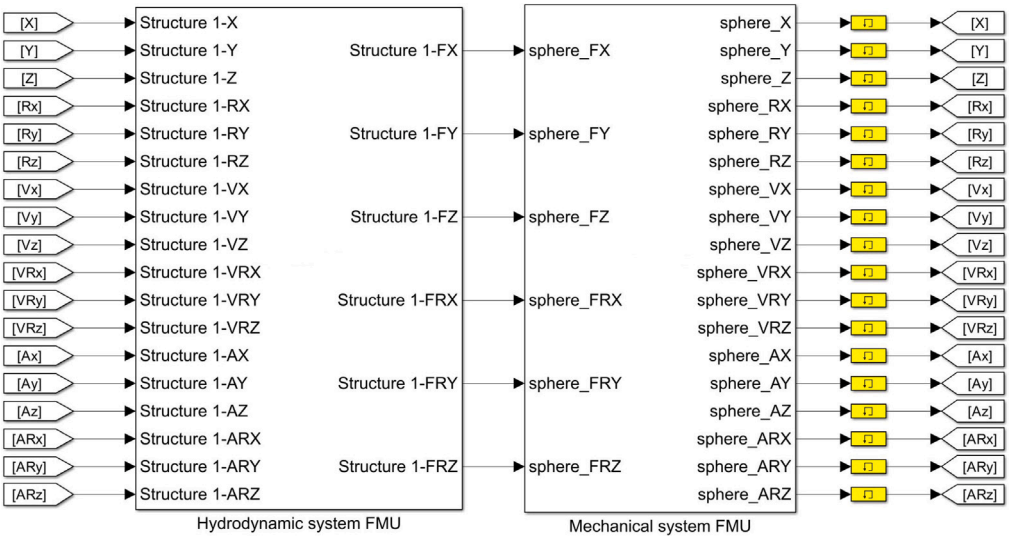

Fig. 4. Co-simulation model of heave decay tests with a floating sphere. The yellow blocks are memory blocks.

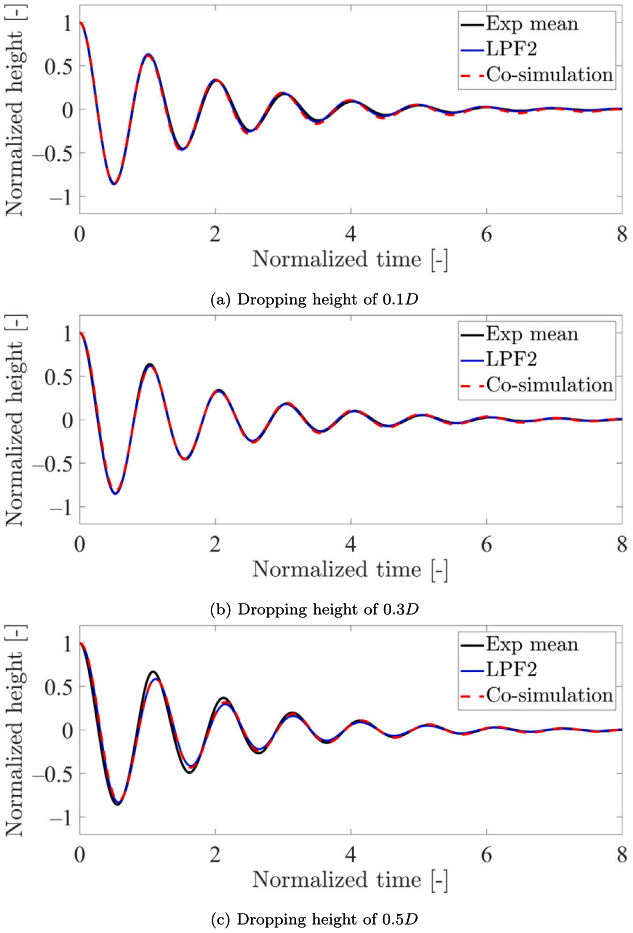

(a) Dropping height of $0.1D$

(b) Dropping height of $0.3D$

(c) Dropping height of $0.5D$

Fig. 5. Normalized decay time series for the three drop heights.

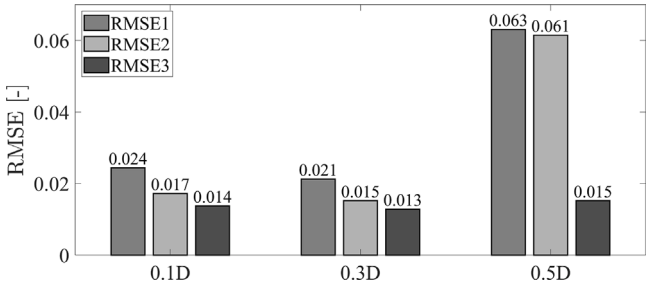

Fig. 6. RMSE between the time series. RMSE1 is the RMSE between the experimental results and the co-simulation results. RMSE2 is the RMSE between the experimental results and the LPF2 results. RMSE3 is the RMSE between the LPF2 results and co-simulation results.

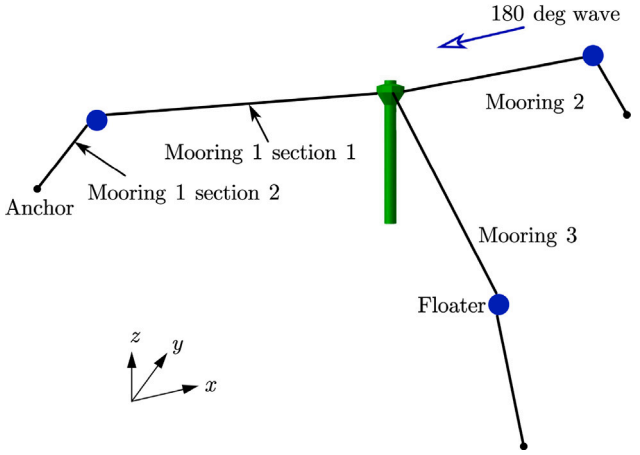

Fig. 7. Diagram of WaveEL 4.0 system regenerated from [59]. The origin is located at the still water surface. The x-axis is aligned with Mooring 2. The wave at 0 deg is aligned with the positive direction of the x-axis.

1 m and a wave period of 6.5 s. The time step is 0.01 s for both models to keep consistency. The waves come from 180 degrees, as indicated in Fig. 7.

Figs. 8 and 9 compare the WEC's motions and the mooring forces from the co-simulation and SESAM model with a time duration of 400 s. It is worth noting that as mooring 1 and mooring 3 are symmetrical around the wave direction, the tension of mooring 1 and mooring 3 are the same. That is why only the tensions of mooring 2 and mooring 3 are shown in Fig. 9. To quantify the difference, Table 3 lists the RMSEs and correlation coefficients between the results from the two models. The correlation coefficients are all close to 1, indicating high correlations between the results. For the heave motion, which is important for the

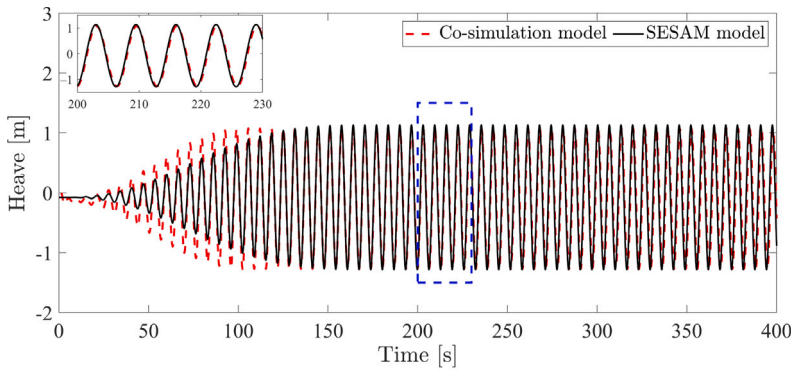

(a) Heave motion

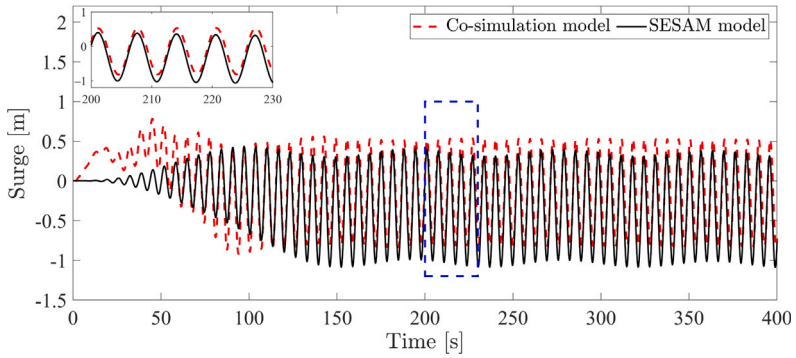

(b) Surge motion

Fig. 8. Heave and surge motions of WaveEL 4.0. The time series with the blue dash line box are zoomed in the upper left corners of each figures.

prediction of power performance for this heaving point absorber, the RMSE is around 5% of the heaving amplitude which is around 2 m, which is deemed as relatively small. Small differences exist between the surge motions of the two models with the RMSE around 14% of their amplitude. This is due to a upward shift of the co-simulation results comparing with the SESAM model. Apart from the shift, their amplitudes are almost the same. Also, considering that the surge motion is not as critical as the heave motion in the prediction of power performance, the differences between the surge motions are deem as within an acceptable range. The shift of the surge motion of the co-simulation results in shift of the mooring forces, as shown in Fig. 9. The RMSEs of mooring 2 and mooring 3 are around 14% and 15% of their amplitudes, respectively. However, unlike the heave and surge motion whose mean values are around 0, the mean value of the mooring tension is around their pretension forces which is around 74 kN. The RMSEs of the mooring tensions are around 6% and 4% of their mean values, which are deemed as small discrepancies. Therefore, by analysing the RMSEs and correlation coefficients between the results from the two models, it is shown that co-simulation can simulate WEC systems containing coupled multiple subsystems and give similar motion and mooring force predictions as the commercial software SESAM.

4. Study case 1 – single NoviOcean WEC

After validating and verifying the co-simulation methodology in Section 3, the NoviOcean WEC is taken as a study case to show the advantages of co-simulations further. This section introduces the modelling approaches of each subsystem of the NoviOcean WEC.

NoviOcean is a multiple-body WEC developed by Novige AB, as shown in Fig. 10. The main components are the piston rod, the water tube, the buoy, and the turbine and generator assembly. The piston rod is anchored to the seabed by a spherical joint. The piston head will pressurize water inside the water tube when the buoy goes up with the waves. The pressurized water will then go through the penstock and flush the turbine on the top. Unlike WaveEL 4.0 which has no direct connection between the buoy and the seabed, the NoviOcean WEC is bottom-fixed to the seabed by the piston rod. Due to the restriction of the bottom-fixed piston rod, the horizontal motion and the heave motion are naturally coupled. The stroke of the piston is designed to be 3 m beyond which the relative velocity between the water tube and the piston is forced to be 0.

4.1. The hydrodynamic and mooring system

Fig. 11 shows the hydrodynamic and mooring system of the NoviOcean WEC. The hydrodynamic system consists of the buoy, the water tube and the piston. The mooring system has four mooring lines. Each has two sections connected by floaters. The main parameters of the hydrodynamic and mooring system are listed in Table 2. The turbine and generator assembly are removed from the model since they are always above the water and do not provide hydrodynamic forces.

4.2. The mechanical system model

The motion mechanism of the piston and the water tube is a modelling challenge, as Ansys Aqwa does not provide such prismatic joints allowing only one translational degree of freedom. In [60], a similar prismatic joint was modelled in WEC-sim and coupled with other subsystem models by Simulink S-function as an interface for the communication between different modules. However, their approach requires programming and is less intuitive than FMU-based co-simulations.

In this study, the prismatic joint is modelled in Ansys Rigid Dynamics, which provides more choices of joints than Ansys Aqwa. The mechanical system is simplified as shown in Fig. 12, ignoring the turbine and generator assembly. The buoy and the water tube are modelled as rigidly fixed to each other. The seabed anchor is modelled by a spherical joint, allowing free rotations.

Table 2
Basic properties of the WaveEL 4.0 and NoviOcean WEC systems.

	Property	WaveEL 4.0	NoviOcean
Hydrodynamic system	Dimension [m]	8.69 (diameter)	38.52; 7.65; 4.65(length, width and height of the buoy)
	Mass [kg]	2.17×10^5	1.82×10^5
	Draft [m]	42	1.25
	Volume $[m^3]$	209.71	175.71
	Centre of gravity, COG_w [m][a]	−10.6	−2.06
	Roll inertia relative to COG_w, I_{xx} $[kg \times m^2]$	5.79×10^7	3.00×10^7
	Pitch inertia relative to COG_w, I_{yy} $[kg \times m^2]$	5.79×10^7	1.25×10^7
	Yaw inertia relative to COG_w, I_{zz} $[kg \times m^2]$	1.47×10^7	1.89×10^7
	Water depth [m]	50	70
Mooring system	Number of mooring lines	3	4
	Mooring system type [–]	Polyester	Polyester
	Fairlead depth below still water line [m]	1	1
	Anchor radius [m]	135.07	122.83
	Unstretched mooring line length [m]	104; 40.7	70;69
	Mooring line diameter [m]	0.08	0.08
	Mooring density [kg/m]	4.9	4.9
	Mooring unstrained axial stiffness $EA_{constant}$ [N]	8538	8538
	Mooring axial stiffness coefficient k_1 [N]	3.00×10^6	3.00×10^6
	Mooring axial stiffness coefficient k_2 [N]	3.00×10^7	3.00×10^7
	Floater structural mass [kg]	2000	2000
	Floater displaced mass of water [kg]	9430	9430
	Floater added mass [kg]	6700	6700
	Drag coefficient times area $[m^2]$	7.35	7.35

[a] The origin of the reference Cartesian coordinate is placed in the plane of the water surface at the geometric centre of the WEC buoy when it is in its unloaded neutral position.

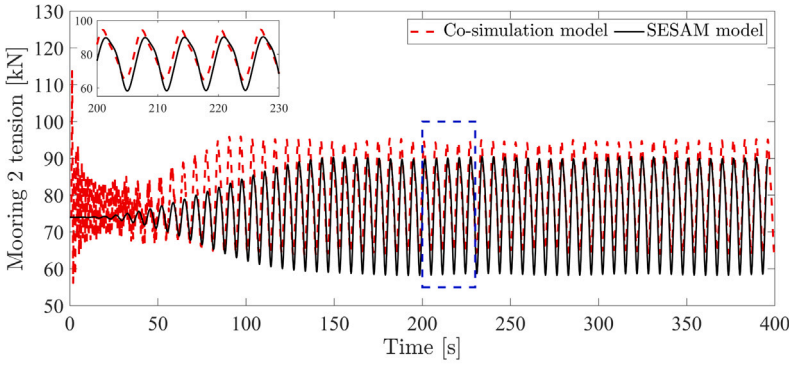

(a) Mooring 2

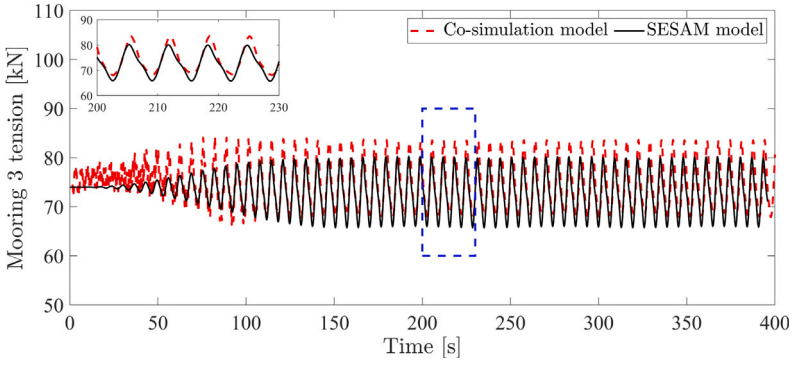

(b) Mooring 3

Fig. 9. Mooring forces of WaveEL 4.0. The time series with the blue dash line box are zoomed in the upper left corners of each figures.

Table 3
RMSMs and correlation coefficients between the results from the co-simulation model and the SESAM model. The analysed time series are after 150 s to avoid the unstable starting phase.

	RMSE	ρ
Heave	0.1177 m	0.9917
Surge	0.2123 m	0.9893
Mooring 2	4.2014 kN	0.9773
Mooring 3	2.6390 kN	0.9719

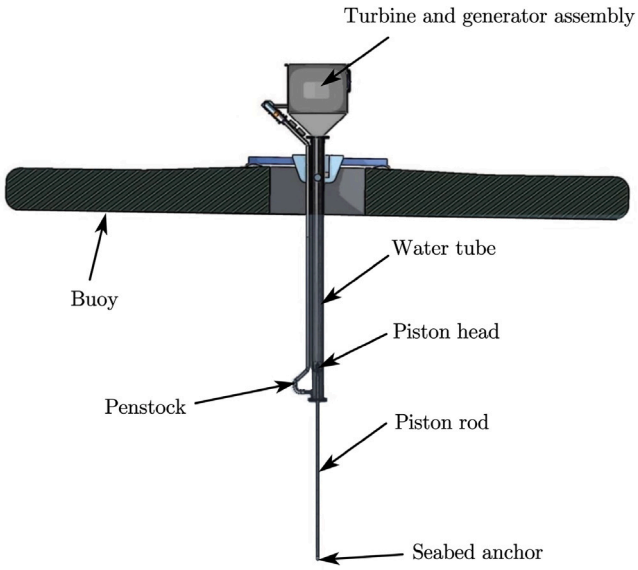

Fig. 10. The NoviOcean WEC.

4.3. The PTO system model

The piston is supposed to pressurize the water to drive the turbine. Integrating the turbine model into the co-simulation is also possible by taking the relative motions between the water tube and the piston as the inputs. However, as the purpose of this study is to demonstrate the capability of the co-simulation and the modelling of a turbine system needs specified expertise, integrating a detailed PTO system will be in our future work. In this paper, the PTO system is instead modelled as a linear damper whose value B_{PTO} is the same as the radiation damping under different wave periods. The intention of selecting the damping coefficient in this way comes from the frequency-domain model described in [61]. The optimal PTO control is a double variable optimization problem which requires two-fold conditions to achieve a maximized power output. The first is that the PTO reactance (K_{PTO}/ω, where K_{PTO} is the PTO stiffness ans ω is the wave angular frequency) must cancel the inherent reactance. However, this condition is hard to achieve since the overall reactance of the whole system is hard to obtain. The second one is that the PTO damping must equal the hydrodynamic radiation damping. In this study, only the second condition is satisfied. Fig. 13 shows the interpolated curve of radiation damping based on BEM results under different wave periods.

In the real proprietary system of NoviOcean WEC, more sophisticated methods, including latching control and optimized ways of restricting the upward motions of the buoy in various wave heights, are used to extract the wave energy with high efficiency. Due to the scope of this paper, the control methods adopted in the real NoviOcean prototype are not included in the PTO system model. Although the PTO system is simplified in this study, the co-simulation model provides great scalability for implementing complex PTO control algorithms in future studies.

4.4. The co-simulation model

The assembled co-simulation model is shown in Fig. 26 in Appendix. A spherical joint element takes the angular rotation velocity in the z direction of the piston as the input and the friction force as output, subtracted from the total force to prevent unwanted yaw motions. The PTO system takes the vertical motion of the buoy as the input and calculates the PTO force using Eq. (4). Then, the PTO force is subtracted from the global vertical force. Simulink handles the communications between different modules at every time step without any explicit programming effort.

5. Study case 2 – 18-WEC wave park

It is necessary to test the capability of co-simulation methodology in simulating large wave parks containing multiple WEC systems. The co-simulation methodology should be able to capture the hydrodynamic interaction effects, as it plays an important role in the overall power performance of a wave park. However, it is worth noting that as there is no experimental data of NoviOcean WECs installed in a wave park, the results of this case cannot be validated in the current stage. The main purpose of this case is to demonstrate the capability of the co-simulation in handling large-scale wave parks numerically. The study case 2 is an 18-WEC wave park consisting of NoviOcean WECs. The layout of the wave park is shown in Fig. 14. Note that the length of the mooring lines is slightly different from the single WEC case, but all other mooring line properties are the same. Also, the piston rod is elongated to cope with the water depth of 70 m in this study case. The separation distance between the WECs in x- and y-axes is 100 m which is chosen to make the wave park compact. The co-simulation model of the 18-WEC wave park is analogous to the single WEC model, as shown in Fig. 26.

6. Results and discussions

This section presents the results and corresponding discussions of the two study cases.

6.1. Study case 1 – single NoviOcean WEC

For the single WEC case, several regular wave sea states with a constant amplitude of 1 m and varying wave periods from 3 s to 11 s were applied to test the motion responses and power performance. Each simulation lasts 400 s and has a time step of 0.1 s. The power performance is computed for the simulation time between 100 s and 400 s when the motion responses are stable.

6.1.1. WEC motions

The relative motion between the buoy and the piston is shown in Fig. 15. It is indicated that the amplitude of relative motion is relevant to the wave period. For short-period waves with periods ranging from 3 s to 7 s, the relative motion amplitude is less than the wave amplitude, which is 1 m. However, for longer period waves, for example, 8–11 s, the relative motion amplitude is similar to the wave amplitude. There are different reasons to explain this phenomenon depending on the wave period. For waves with very short periods, 3 s or 4 s, the WEC buoy cannot follow the rapidly changing wave excitation force, resulting in small relative motion amplitudes. For waves with periods from 5 s to 7 s, the relative motion smaller than 1 m is mainly due to the relatively large surge motions. It is shown in Fig. 16 that under the waves with period of 5 s, the WEC's largest surge motion can be up to 9 m. As the wave periods increase from 5 s, the surge motion reduces. For longer wave periods from 9 s to 11 s, the surge motion is within −2 m to 2 m. The prismatic joint between the buoy and the piston results in the coupled heave and surge motion, which means that large surge motions reduce the amplitude of heave motions. This emphasizes the necessity of modelling the WEC using a co-simulation approach to consider such a prismatic joint.

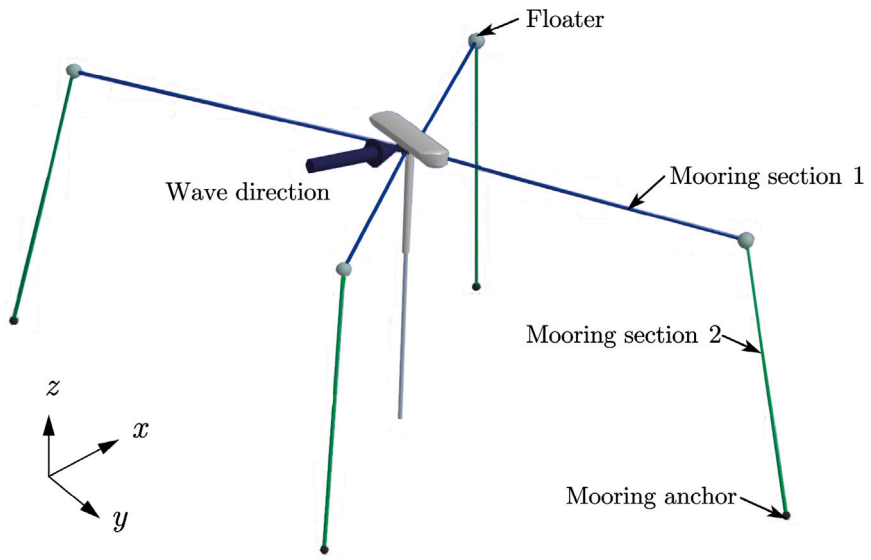

Fig. 11. The hydrodynamic and mooring system of the NoviOcean WEC. The origin is located at the still water surface. The wave direction is at 0 deg which is aligned with the positive direction of the x-axis. The angle between each mooring and the x-axis is 60 deg.

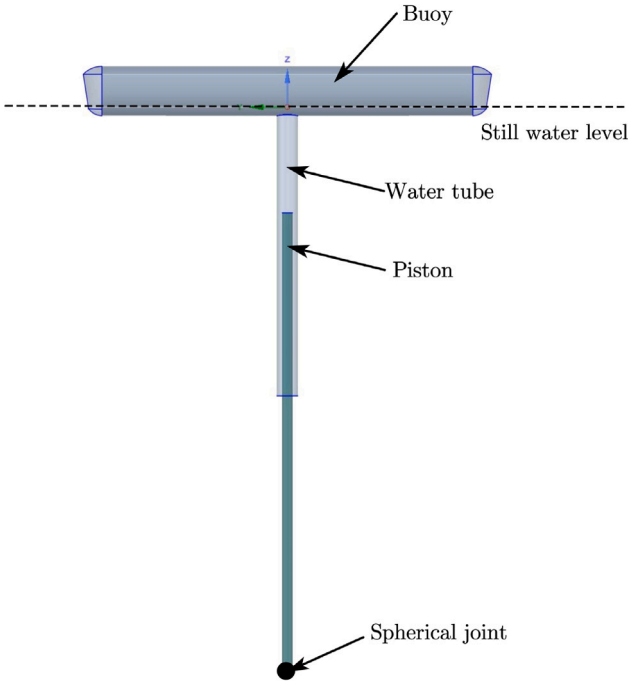

Fig. 12. The simplified mechanical model of the NoviOcean WEC. The prismatic joint refers to the connection between the piston and the water tube which only allows translation along the common axis.

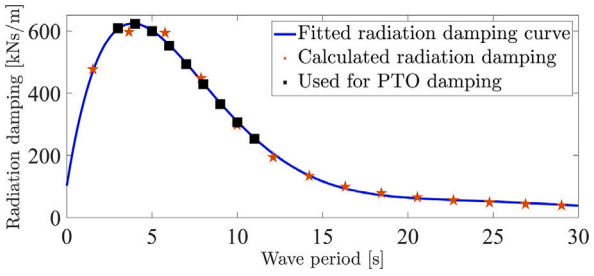

Fig. 13. The radiation damping of the NoviOcean WEC.

6.1.2. Power performance

The power performance of a single WEC is computed using Eq. (5) and shown in Fig. 17 for regular waves with different periods. There is a mismatch between the peaks of PTO damping and averaged power performance, as the largest PTO damping is for a wave period of 4 s while the largest averaged power performance happens for a wave period of 5 s. The explanation for this mismatch is that including the mooring system introduces nonlinear stiffness that affects the dynamic responses of the WEC and, consequently, the power performance. It indicates that even for regular waves, to get a more accurate power performance prediction, it is necessary to simulate WECs in the time domain instead of the frequency domain if the mooring system is included.

6.2. Study case 2 – 18-WEC wave park

A series of irregular wave sea states are tested for the 18-WEC wave park to represent the real physical environments. The irregular waves follow the JONSWAP spectrum defined by significant wave height H_s, peak period T_p and peak enhancement factor γ. The value used for the empirical parameter γ is 2.4. With a fixed peak period of 9 s, three significant wave heights, 0.9, 1.8 and 2.7 m, combined with three wave directions, 0, 12 and 24 degrees, are tested to analyse these factors' influence on dynamic responses and power performance of each WEC within the 18-WEC wave park. The irregular wave parameters are listed in Table 4 for clarity. All the simulations have a duration of 1800 s. The time step is 0.1 s which can capture the transient responses of the WECs with satisfactory accuracy.

6.2.1. WEC motions

The contour of surge-heave trajectories of each WEC within the wave park under different significant wave heights are shown in Figs. 18–20. The contours represent the motion range of each WEC within the vertical plane. The purpose the figures is to show the motion patterns of each WEC and visualize the influence of the interaction effects under different sea states.

The factors vary in Figs. 18–20 are the wave heights and wave directions. It is observed that the amplitude of the heave motion of each WEC shows clear relevance to the wave height. From Figs. 18 to 20, the wave height increases from 0.9 m to 2.7 m. As the wave height increases, the amplitude of the heave motion also increases. The range of the surge motions is observed to be saturated when the significant

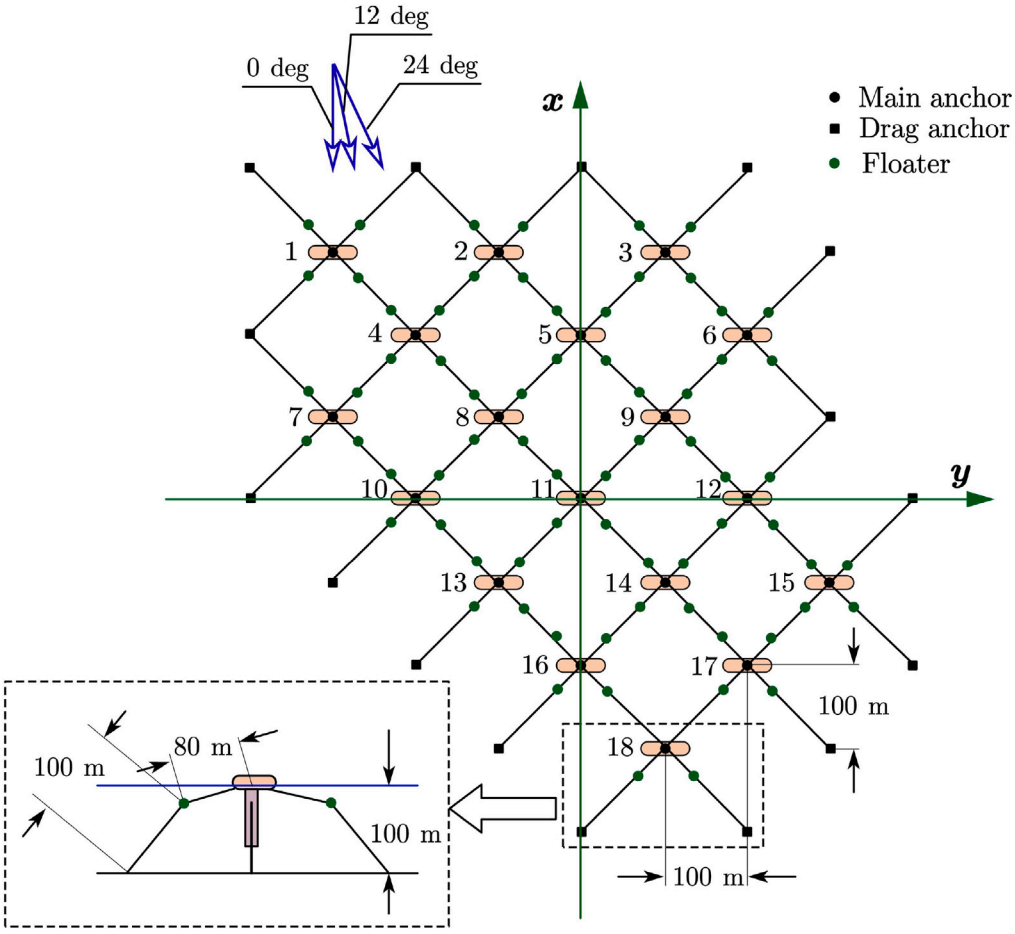

Fig. 14. 18-WEC wave park with a WEC distance of 100 m.

Table 4
Parameters of the simulated irregular wave sea states in study case 2.

Sea states	Significant wave height H_s [m]	Peak period T_p [s]	Directions [deg]
1	0.9	9	0
2	0.9	9	12
3	0.9	9	24
4	1.8	9	0
5	1.8	9	12
6	1.8	9	24
7	2.7	9	0
8	2.7	9	12
9	2.7	9	24

wave height increases from 1.8 m to 2.7 m, with the largest surge range (−20 m to 5 m) happening in the first line of the WECs. This can be explained by the restrictions of the mooring system. The influence of changing wave directions is mainly on the range of the surge motion, as it is observed that the range of the heave motion remains almost unchanged with varying wave direction for each WEC within the wave park.

The diffraction effect, which is a part of the interaction effects, is observed as the WECs in the front of the wave park generally suffer a higher surge motion than the WECs in a relatively backward position. It proves that the co-simulation model can capture the interaction effects between multiple WECs. The influence of interaction effects on the heave motion is not obvious, as the ranges of the heave motion are similar for each WEC.

The contour of surge-sway trajectories of each WEC under a significant wave height of 1.8 m are shown in Fig. 21. The surge-sway trajectories tilt accordingly as the wave direction changes from 0 to 12 and finally to 24 degrees. Meanwhile, the range of the sway motion tends to increase as the wave direction tilts more. It indicates that the features of the spherical joints are represented properly by the co-simulation model.

Overall, from the WEC motion results, it is shown that the co-simulation model of the 18-WEC wave park properly integrates the effect of the mooring system and interaction between the WECs into the global simulation.

6.2.2. *WEC performances*

The power performance of a WEC within the wave park is calculated the same way as for a single WEC. As the tested irregular sea states

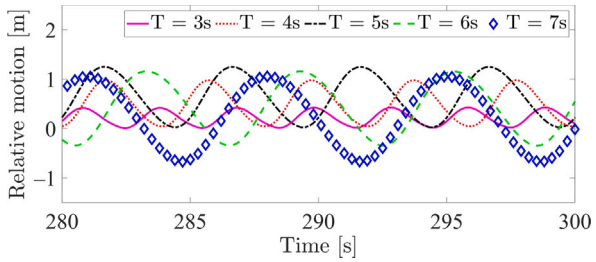

(a) Wave period from 3 s to 7 s.

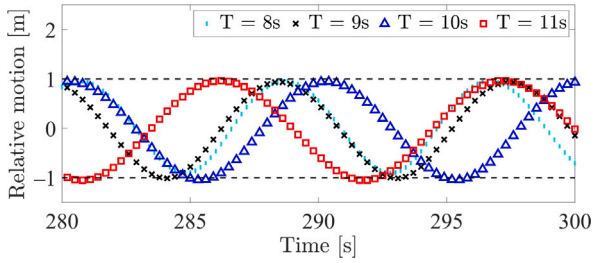

(b) Wave period from 8 s to 11 s.

Fig. 15. Relative motions between the buoy and the piston under regular waves with an amplitude of 1 m and varying wave periods. The black dashed lines indicate the range of wave elevation.

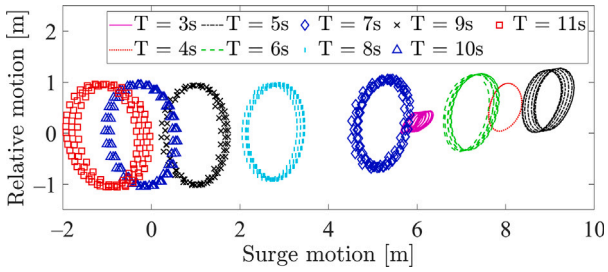

Fig. 16. The surge motions versus the relative motion between the buoy and the piston.

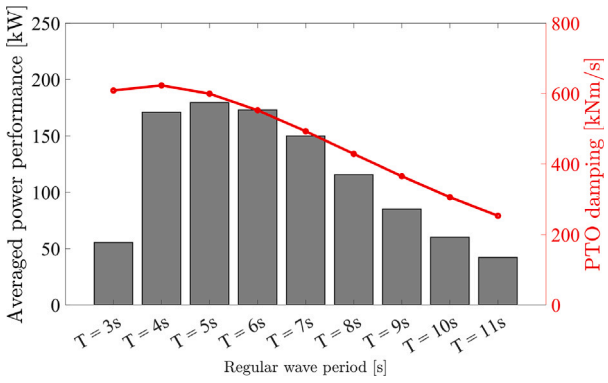

Fig. 17. The averaged power performance of the WEC under regular waves with a constant wave amplitude of 1 m and varying wave periods.

share the same wave period of 9 s, the PTO damping value is chosen as 365 kN s/m for all the WECs under all tested sea states. This damping value is chosen from the fitted radiation damping curve in Fig. 13 at wave period of 9 s.

Fig. 22 shows the power performance of each WEC under three different wave heights. The upstream WECs of the wave park tend to outperform the downstream WECs for all three sea states. Compared with the power performance of a single WEC, it is observed that the upstream WECs produce more power while for the downstream WECs, their power performance can be lower than an isolated WEC. The increased power performance of the upstream WECs can be explained by the radiated waves from the downstream WECs. However, for the downstream WECs, the diffraction effect caused by the WECs in the front is severe as observed from Figs. 18–20, which results in smaller power absorption.

It is worth noting that the result should be analysed with extra caution for the case with H_s = 2.7 m. This is because, at that wave height, the WEC motions are large, especially in the vertical direction, as shown in Fig. 20. It means that the linear potential theory may not be applicable since the small motion assumption may be violated. Fortunately, as the nonlinear hydrostatic force is fully considered in the hydrodynamic model and the simulation results of the nonlinear heave decay test show good agreement with the experiment in Fig. 5, the results of the largest wave height can be trusted with cautions.

With changing wave directions, the power performance of each WEC changes slightly, as shown in Fig. 23. For most of the WECs except a few in the downstream, their power performances tend to outperform the corresponding single isolated WEC. This wave park's most favourable wave direction is 12 degrees, under which most WECs show better power performance than the other two wave directions. This is due to the yaw-rotation feature of the WEC, which can be captured properly by the co-simulation model. For the 12 degrees wave direction, each WEC rotates to be perpendicular to the incoming waves. After rotations, this new wave park layout results in more positive interactions between WECs than for the other two wave directions. Similar trends can be observed for different wave heights whose figures are not shown.

The total power performance of a wave park is an important factor to be considered before the real installation. Fig. 24 shows the total performance under all tested sea states. Compared with the power performance of 18 isolated WECs, this wave park shows power increases due to the interaction effects. The largest percentage of power increase can be up to 36%. Among the three wave directions, 12 degrees is the optimum, enabling the largest power performance.

As mentioned in Section 4.3, the control methods adopted in the NoviOcean WEC are not modelled in detail in this study. Therefore, the power performance predictions provided by the co-simulation model are smaller than the real NoviOcean WEC. Nevertheless, the NoviOcean team states the interaction results and the relative performance increases relative to the wave direction likely correspond closely to the real scenario.

6.3. Computation time

The main hydrodynamic computation for the co-simulation has two parts. The first part is the calculation of the hydrodynamic coefficients in the frequency domain, which only needs to be done once and can be reused. The second part is the calculation of the hydrodynamic and non-linear hydrostatic forces in the time domain based on the instantaneous motions of WECs. The computation time needed for the hydrodynamic coefficient calculation is about 15 min for study case 2 with 33 392 mesh elements when running Ansys Aqwa on a computer equipped with an Intel(R) Core(TM) i9-10900 CPU with a clock speed of 2.81 GHz. The time domain calculation of the hydrodynamic and hydrostatic forces is coupled with the mooring force calculation, making it time-consuming. The overall solving time of the co-simulation, excluding the hydrodynamic coefficient calculation, is about 4 h for study case 2, with a simulation time of 1800 s. The current computation time is comparable to a similar simulation running in SESAM. It indicates that co-simulation, as a new framework, can provide a more accurate and flexible modelling approach without increasing computation time.

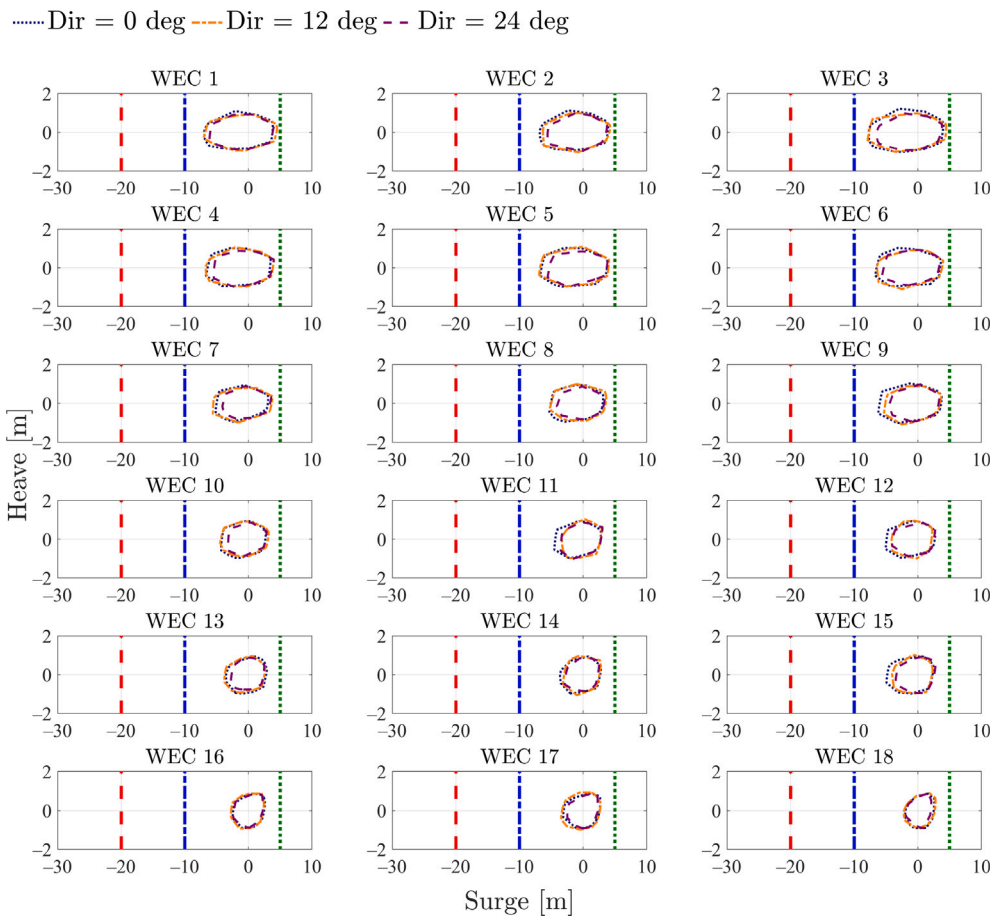

Fig. 18. The contour of surge-heave trajectories of the WECs under waves of H_s = 0.9 m, T_p = 9 s. The vertical straight lines work as gauges to make it easier to compare the surge motion ranges with other sea states.

7. Conclusions

This study presents an FMI-based co-simulation framework which is suitable for WEC system simulations. This framework enables separate modelling of each subsystem in different computer programs to fulfil different modelling requirements. The subsystem models can then be coupled together to constitute a global model in a unified environment. The co-simulation framework is based on the FMI standard and co-simulation algorithm. The FMI standard defines the communication interface between a model and a simulation environment, and the co-simulation algorithm is responsible for managing the communication between different models and advancing the global simulation.

A WEC system consists of different subsystems which need to be modelled using knowledge from different areas. It can be divided into four subsystems: hydrodynamic, mooring, mechanical, and PTO system. In this study, the hydrodynamic and mooring systems were modelled together using Ansys Aqwa. The mechanical system model was built in Ansys Rigid Dynamics. The PTO system was modelled directly in Simulink. The first two models were exported as FMUs, encapsulating model information and solvers. The co-simulation model was built by importing each FMU to Simulink and connecting corresponding input/output pins. Compared with the conventional WEC simulations carried out in a single software, the FMI-based co-simulation is advantageous in the following aspects:

- The mechanical system can be better simulated using a broader range of joints and constrictions provided by Ansys Rigid Dynamics.
- The PTO system can be modelled in a more flexible way. Possible PTO control algorithms can be easily applied to a co-simulation model in the Simulink environment.

Moreover, the coupling of different solvers can be taken care of by a platform providing the co-simulation algorithm, which in this study is Simulink. No further programming effort is needed. This can free engineers from programming-related issues and make the co-simulation framework highly suitable for the development phase of a WEC system, which requires a fast modelling iteration process.

In this study, the FMI-based co-simulation framework is validated by an experimental heave decay test and verified by a numerical WEC system model in a code-to-code way. Two study cases of the NoviOcean WEC were simulated under regular and irregular waves. Study case 1 tested a single NoviOcean WEC. Study case 2 is a wave park consisting of 18 WECs. The main findings are listed as follows:

- For a single WEC under regular waves, the amplitude of the relative motion between the buoy and the piston is closely related to wave periods. The largest averaged power performance happens for a wave period of 5 s. Modelling the prismatic joint between the buoy and piston is essential to obtain reasonable results.
- For the 18-WEC wave park, the interaction effects between the WECs have a complex influence on each WEC. The surge motions of the downstream WECs decrease due to the diffraction effects from the upstream WECs. The power performance of each WEC gets a positive or negative effect depending on its location in the wave energy park and the wave directions.

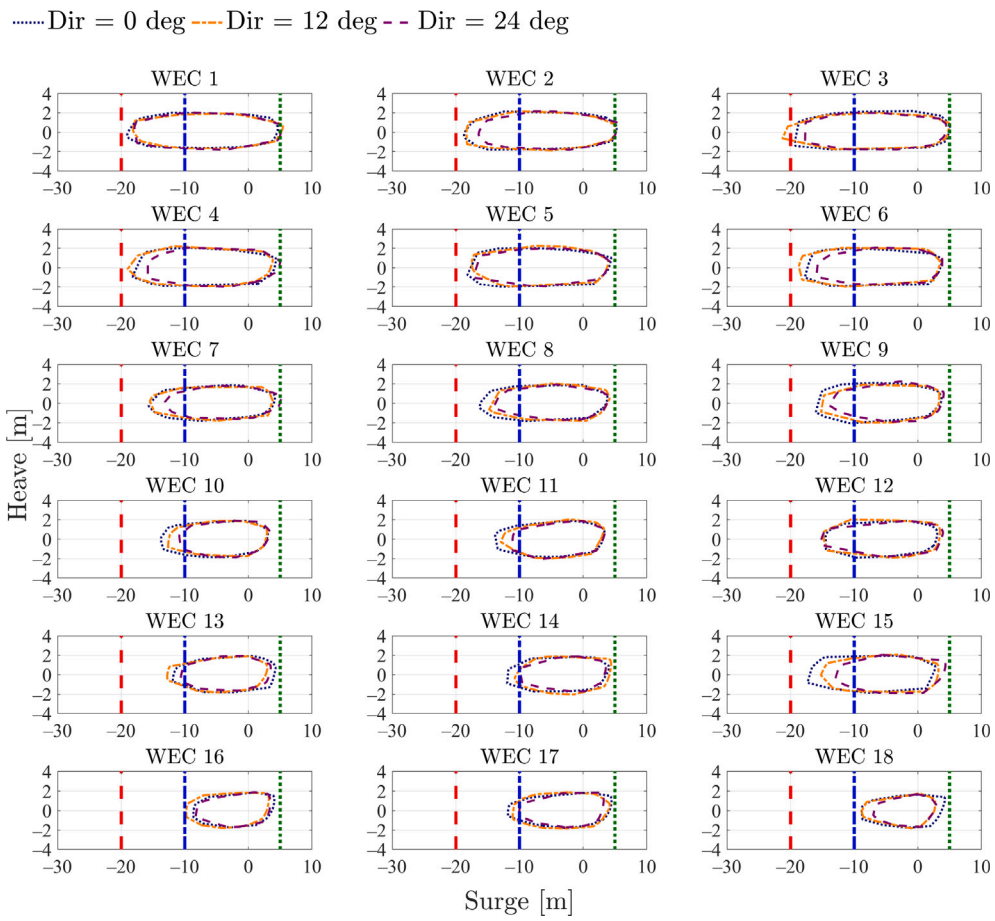

Fig. 19. The contour of surge-heave trajectories of the WECs under waves of H_s = 1.8 m, T_p = 9 s. The vertical straight lines work as gauges to make it easier to compare the surge motion ranges with other sea states.

- Among the tested three wave directions, 12 degrees is the best one for the 18-WEC wave park, resulting in the largest total power performance.
- The total power performance of the wave park gets improved by the interaction effects under all tested sea states, and the largest improvement is 36% compared with an isolated WEC unit under the same sea state.

Overall, the FMI-based co-simulation can handle simulations of single WEC systems and multiple WEC wave parks with hydrodynamic, mechanical, mooring and PTO subsystems considered. Its simplicity and flexibility make it promising in the WEC design and simulation. In the future work, the detailed PTO system model including explicit component model and control law will be integrated to better estimated the power performance of WEC systems.

CRediT authorship contribution statement

Xinyuan Shao: Writing – review & editing, Writing – original draft, Visualization, Validation, Software, Methodology, Investigation, Formal analysis, Conceptualization. **Jonas W. Ringsberg:** Writing – review & editing, Supervision, Resources, Project administration, Funding acquisition, Conceptualization. **Erland Johnson:** Writing – review & editing, Supervision, Conceptualization. **Zhiyuan Li:** Writing – review & editing, Supervision, Conceptualization. **Hua-Dong Yao:** Writing – review & editing, Supervision, Conceptualization. **Jan G. Skjoldhammer:** Writing – review & editing, Supervision, Conceptualization. **Stefan Björklund:** Writing – review & editing, Supervision, Conceptualization.

Declaration of competing interest

The authors declare that they have no known competing financial interests or personal relationships that could have appeared to influence the work reported in this paper.

Acknowledgements

This work was performed within the projects ‘Control of wave energy converters based on wave measurements, for optimal energy absorption’, funded by the Swedish Energy Agency through contract agreement no. 50197-1, and ‘INTERACT Analysis of array systems of wave energy converters with regard to interaction effects in the LCoE and fatigue analyses’, funded by the Swedish Energy Agency through contract agreement no. 50148-1. This work also received funding from the Chalmers University of Technology Foundation for the strategic research project ‘Hydro- and aerodynamics’.

Appendix

See Figs. 25 and 26.

Data availability

Data will be made available on request.

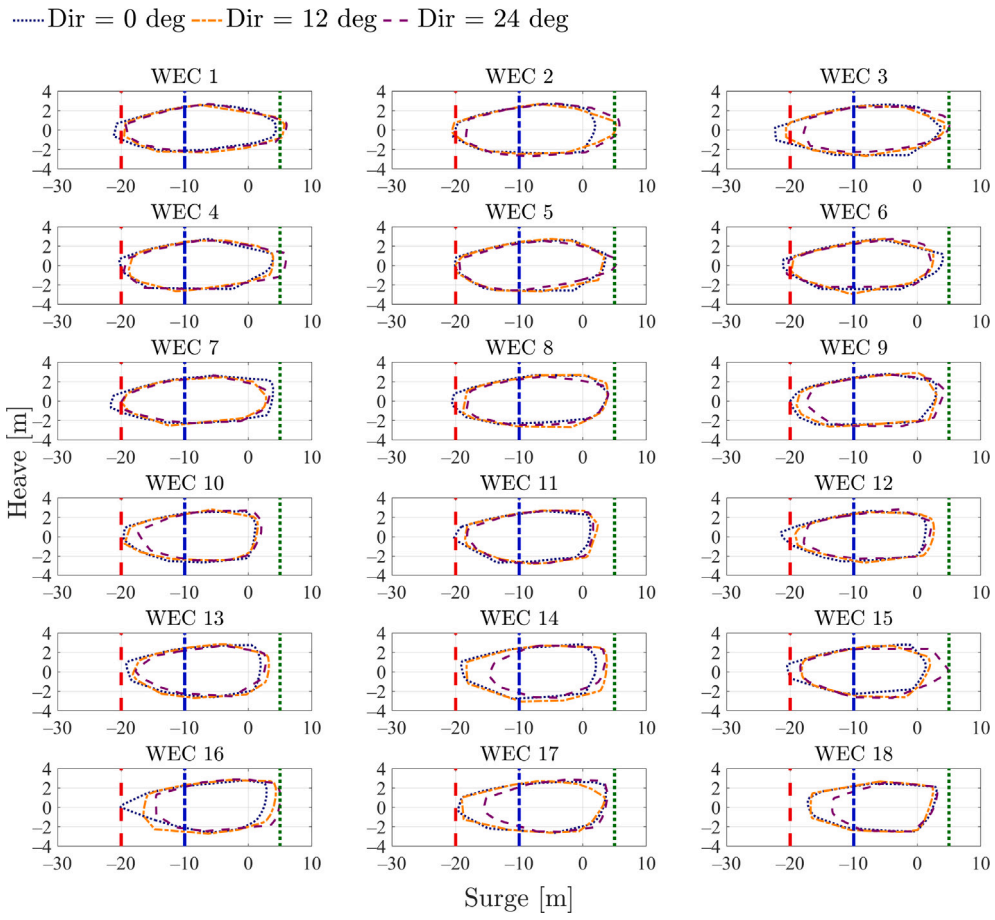

Fig. 20. The contour of surge-heave trajectories of the WECs under waves of H_s = 2.7 m, T_p = 9 s. The vertical straight lines work as gauges to make it easier to compare the surge motion ranges with other sea states.

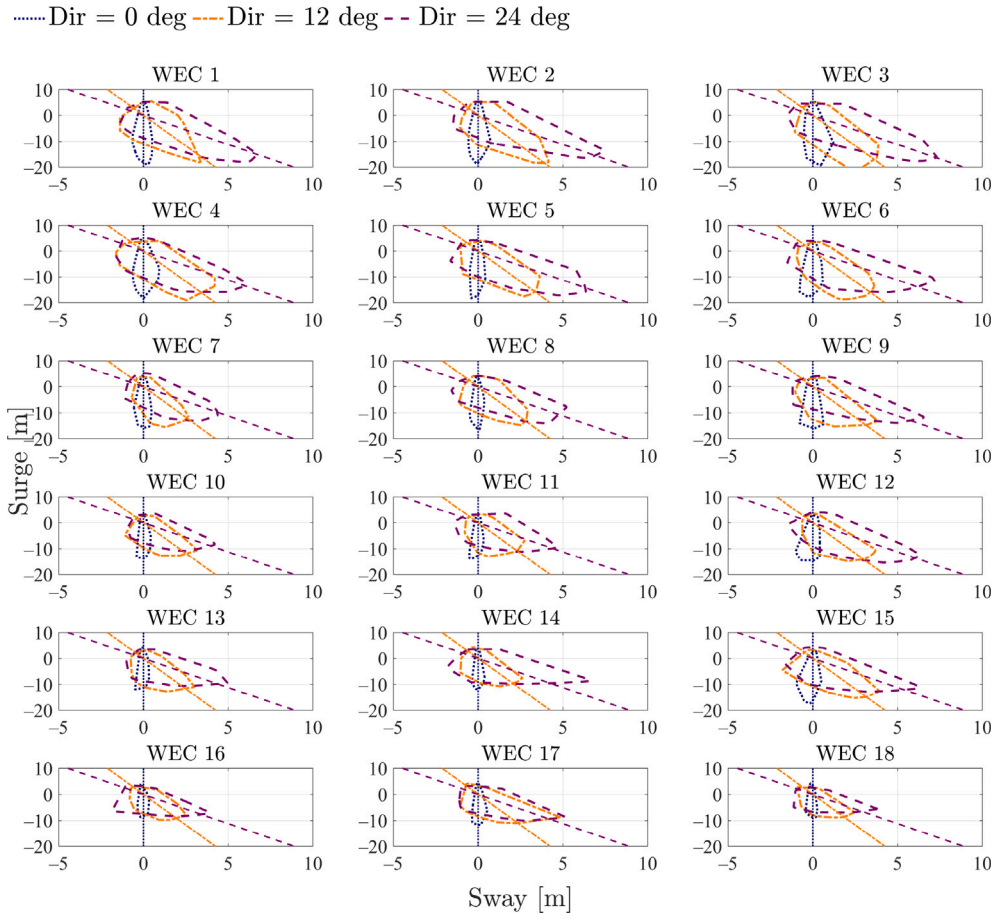

Fig. 21. The contour of surge-sway trajectories of the WECs under H_s = 1.8 m, T_p = 9 s. The straight lines indicate 0, 12 and 24 degrees.

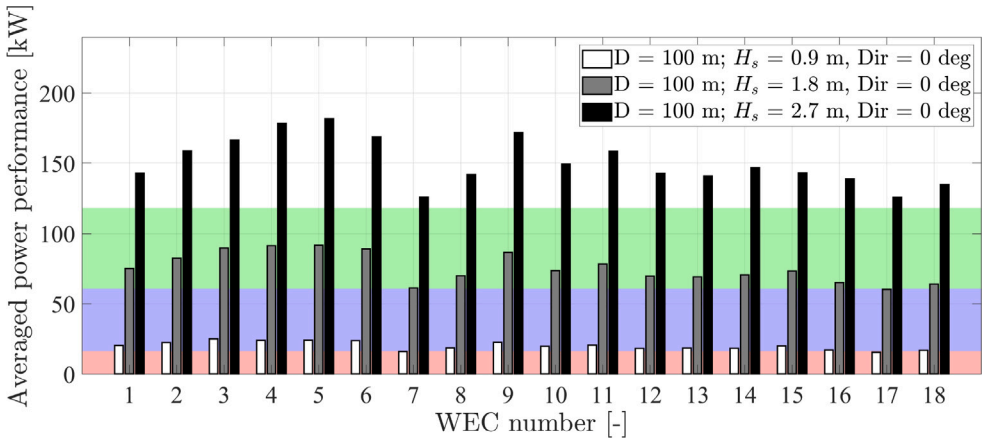

Fig. 22. Power performance of each WEC under changing wave height. The upper range of the red, blue and green background indicates the power performance of a single isolated WEC under the three sea states.

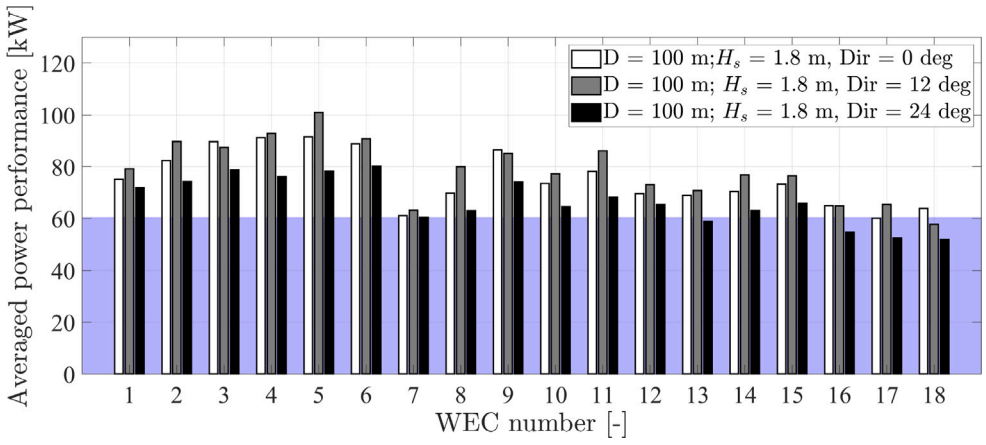

Fig. 23. Power performance of each WEC under changing wave direction. The upper range of the blue background indicates the power performance of a single WEC under waves of H_s = 1.8 m coming from 0 deg.

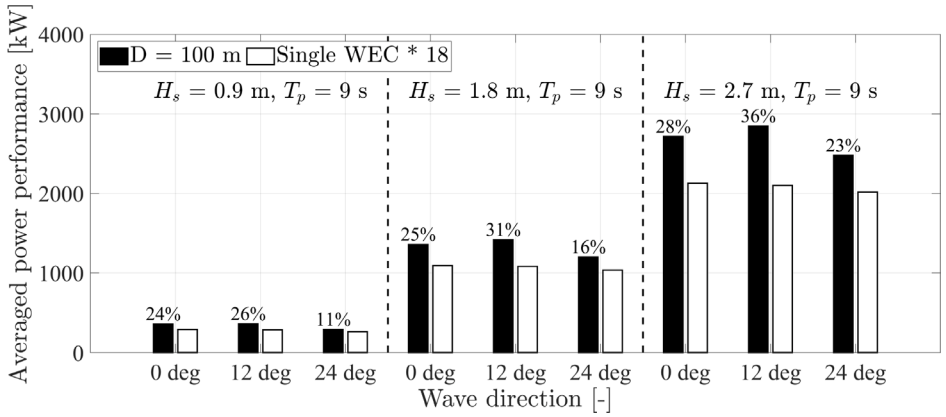

Fig. 24. Total power performance. The percentages indicate the power increase compared with an isolated single WEC.

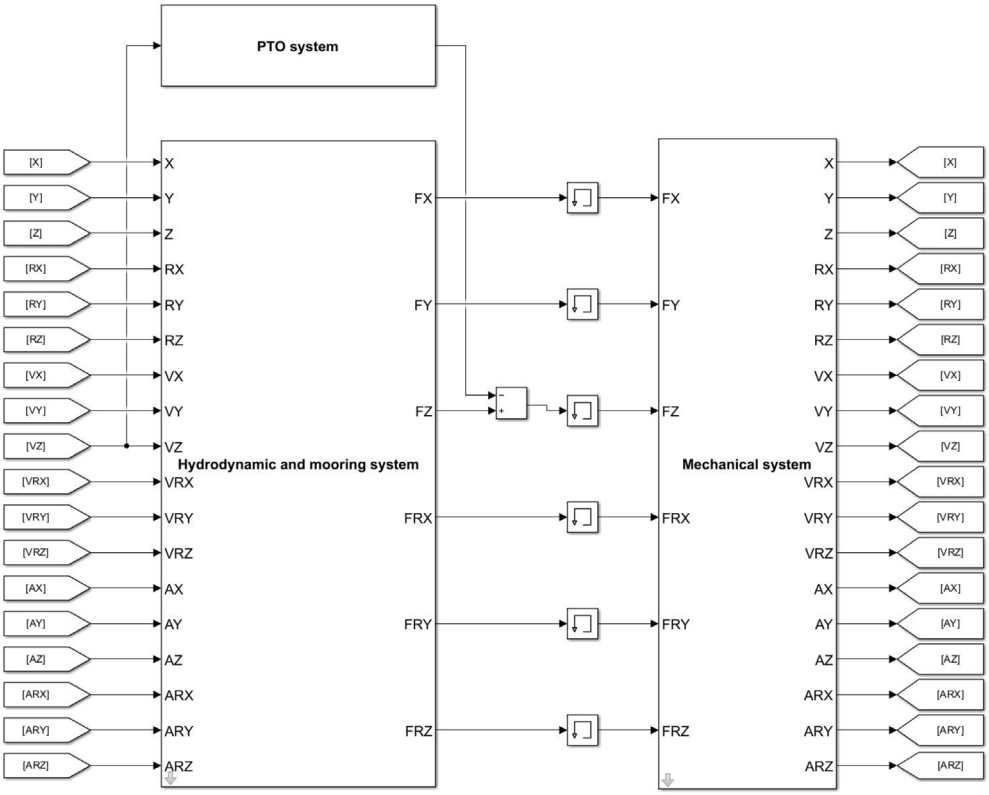

Fig. 25. Co-simulation model of WaveEL 4.0.

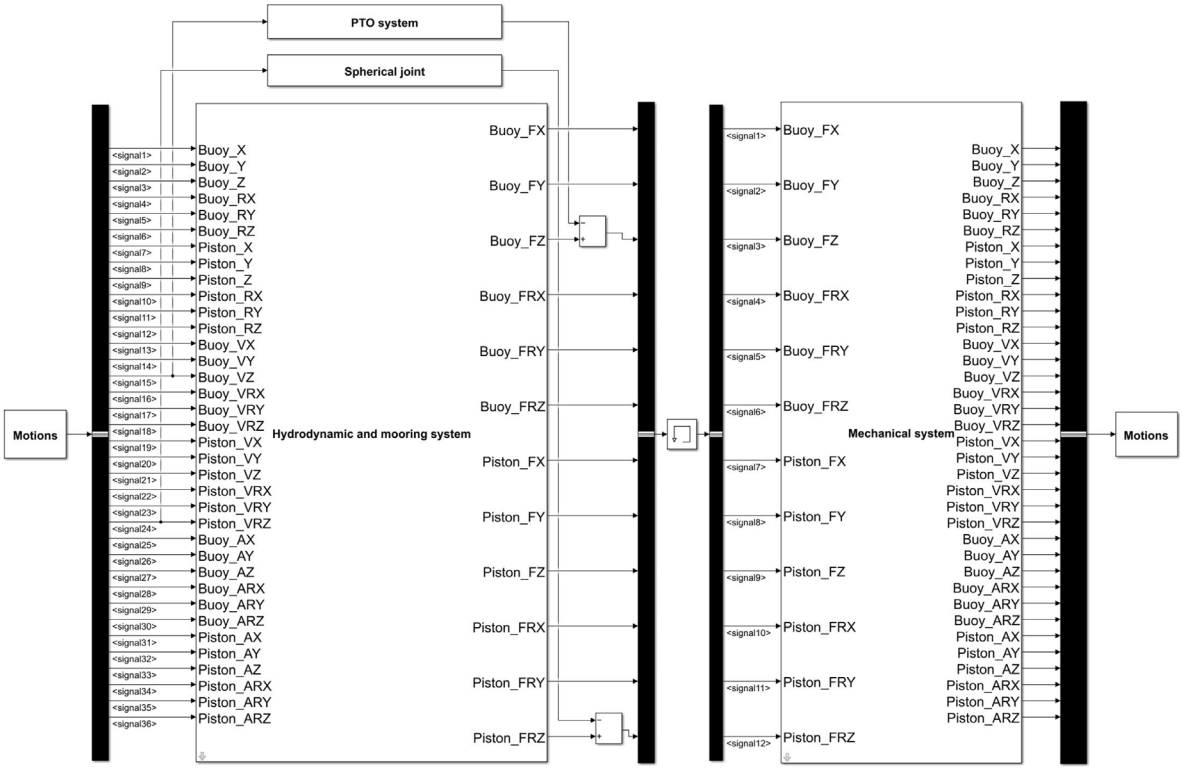

Fig. 26. Co-simulation model of a single NoviOcean WEC.

References

[1] Thorpe TW, et al. A brief review of wave energy. In: A report produced for the UK Department of Energy. Report No ETSU–120, 1999.

[2] Clément A, McCullen P, Falcão A, Fiorentino A, Gardner F, Hammarlund K, Lemonis G, Lewis T, Nielsen K, Petroncini S, et al. Wave energy in Europe: current status and perspectives. Renew Sustain Energy Rev 2002;6(5):405–31. http://dx.doi.org/10.1016/S1364-0321(02)00009-6.

[3] Falnes J. A review of wave-energy extraction. Mar Struct 2007;20(4):185–201. http://dx.doi.org/10.1016/j.marstruc.2007.09.001.
[4] Falcao AFdO. Wave energy utilization: A review of the technologies. Renew Sustain Energy Rev 2010;14(3):899–918.
[5] Ansys Inc. Ansys Aqwa. 2023, URL https://www.ansys.com/products/fluids/ansys-aqwa Version 2023 R1.
[6] DNV GL. SESAM. 2023, URL https://sesam.dnv.com/.
[7] Orcina. OrcaFlex. 2023, URL https://www.orcina.com/orcaflex/ Version 11.1a.
[8] Yang S-H, Ringsberg JW, Johnson E. Parametric study of the dynamic motions and mechanical characteristics of power cables for wave energy converters. J Mar Sci Technol 2017;23(1):10–29. http://dx.doi.org/10.1007/s00773-017-0451-0.
[9] Yang S-H, Ringsberg JW, Johnson E. Wave energy converters in array configurations—Influence of interaction effects on the power performance and fatigue of mooring lines. Ocean Eng 2020;211:107294. http://dx.doi.org/10.1016/j.oceaneng.2020.107294.
[10] Pastor J, Liu Y. Frequency and time domain modeling and power output for a heaving point absorber wave energy converter. Int J Energy Environ Eng 2014;5(2):101. http://dx.doi.org/10.1007/s40095-014-0101-9.
[11] Lee H, Poguluri S, Bae Y. Performance analysis of multiple wave energy converters placed on a floating platform in the frequency domain. Energies 2018;11(2):406. http://dx.doi.org/10.3390/en11020406.
[12] Chen W, Wu Z, Liu J, Jin Z, Zhang X, Gao F. Efficiency analysis of a 3-DOF wave energy converter (SJTU-WEC) based on modeling, simulation and experiment. Energy 2021;220. http://dx.doi.org/10.1016/j.energy.2020.119718.
[13] Shi Q, Xu D, Zhang H. Performance analysis of a raft-type wave energy converter with a torsion bi-stable mechanism. Energy 2021;227. http://dx.doi.org/10.1016/j.energy.2021.120388.
[14] Xiao H, Liu Z, Zhang R, Kelham A, Xu X, Wang X. Study of a novel rotational speed amplified dual turbine wheel wave energy converter. Appl Energy 2021;301. http://dx.doi.org/10.1016/j.apenergy.2021.117423.
[15] Chen S, Jiang B, Li X, Huang J, Wu X, Xiong Q, Parker RG, Zuo L. Design, dynamic modeling and wave basin verification of a hybrid wave–current energy converter. Appl Energy 2022;321. http://dx.doi.org/10.1016/j.apenergy.2022.119320.
[16] Bao X, Li F, Sun H, Iglesias G, Shi H. Performance characteristics and parameter analysis of a multi-DOF wave energy converter with hybrid power take-off systems. Energy Convers Manage 2023;278. http://dx.doi.org/10.1016/j.enconman.2023.116751.
[17] Chen W, Lu Y, Li S, Gao F. A bio-inspired foldable-wing wave energy converter for ocean robots. Appl Energy 2023;334. http://dx.doi.org/10.1016/j.apenergy.2023.120696.
[18] He G, Liu C, Zhang W, Luan Z, Zhang Z. Numerical study of the effect of central platform motion on the wave energy converter array. Ocean Eng 2023;286. http://dx.doi.org/10.1016/j.oceaneng.2023.115483.
[19] Zhang J, Zhao X, Greaves D, Jin S. Modeling of a hinged-raft wave energy converter via deep operator learning and wave tank experiments. Appl Energy 2023;341. http://dx.doi.org/10.1016/j.apenergy.2023.121072.
[20] Gao H, Xiao J, Liang R. Capture mechanism of a multi-dimensional wave energy converter with a strong coupling parallel drive. Appl Energy 2024;361. http://dx.doi.org/10.1016/j.apenergy.2024.122828.
[21] Han Z, Cao F, Tao J, Zhang C, Shi H. Study on the energy capture spectrum (ECS) of a multi-DOF buoy with MMR-PTO damping. Ocean Eng 2024;294. http://dx.doi.org/10.1016/j.oceaneng.2024.116698.
[22] Wang Y, Shi W, Michailides C, Wan L, Kim H, Li X. WEC shape effect on the motion response and power performance of a combined wind-wave energy converter. Ocean Eng 2022;250. http://dx.doi.org/10.1016/j.oceaneng.2022.111038.
[23] Yazdi H, Ghafari HR, Ghassemi H, He G, Karimirad M. Wave power extraction by Multi-Salter's duck WECs arrayed on the floating offshore wind turbine platform. Energy 2023;278. http://dx.doi.org/10.1016/j.energy.2023.127930.
[24] Zhou B, Hu J, Jin P, Sun K, Li Y, Ning D. Power performance and motion response of a floating wind platform and multiple heaving wave energy converters hybrid system. Energy 2023;265. http://dx.doi.org/10.1016/j.energy.2022.126314.
[25] Chen Z, Sun J, Yang J, Sun Y, Chen Q, Zhao H, Qian P, Si Y, Zhang D. Experimental and numerical analysis of power take-off control effects on the dynamic performance of a floating wind-wave combined system. Renew Energy 2024;226. http://dx.doi.org/10.1016/j.renene.2024.120353.
[26] Wei ZW, Shi HD, Cao FF, Yu MQ, Li M, Chen Z, Liu P. Study on the power performance of wave energy converters mounted around an offshore wind turbine jacket platform. Renew Energy 2024;221. http://dx.doi.org/10.1016/j.renene.2023.119786.
[27] Li X, Xiao Q, Zhou Y, Ning D, Incecik A, Nicoll R, McDonald A, Campbell D. Coupled CFD-MBD numerical modeling of a mechanically coupled WEC array. Ocean Eng 2022;256:111541. http://dx.doi.org/10.1016/j.oceaneng.2022.111541.
[28] Zhang Y, Zhao Y, Sun W, Li J. Ocean wave energy converters: Technical principle, device realization, and performance evaluation. Renew Sustain Energy Rev 2021;141. http://dx.doi.org/10.1016/j.rser.2021.110764.
[29] Liu Z, Zhang R, Xiao H, Wang X. Survey of the mechanisms of power take-off (PTO) devices of wave energy converters. Acta Mech Sin 2020;36(3):644–58. http://dx.doi.org/10.1007/s10409-020-00958-z.
[30] Gallutia D, Tahmasbi Fard M, Gutierrez Soto M, He J. Recent advances in wave energy conversion systems: From wave theory to devices and control strategies. Ocean Eng 2022;252. http://dx.doi.org/10.1016/j.oceaneng.2022.111105.
[31] Zhou Y, Liu H, Kong F, Wang X, Jin Y, Sun C, Chen H. Research on the design and optimal control of the power take-off (PTO) system for underwater eel-type power generators. Appl Energy 2024;372. http://dx.doi.org/10.1016/j.apenergy.2024.123845.
[32] Zeinali S, Wiktorsson M, Forsberg J, Lindgren G, Lindström J. Optimizing the hydraulic power take-off system in a wave energy converter. Ocean Eng 2024;310. http://dx.doi.org/10.1016/j.oceaneng.2024.118636.
[33] Liu C, Hu M, Gao W, Chen J, Zeng Y, Wei D, Yang Q, Bao G. A high-precise model for the hydraulic power take-off of a raft-type wave energy converter. Energy 2021;215. http://dx.doi.org/10.1016/j.energy.2020.119107.
[34] Masoomi M, Sarlak H, Rezanejad K. Hydrodynamic performance analysis of a new hybrid wave energy converter system using OpenFOAM. Energy 2023;269. http://dx.doi.org/10.1016/j.energy.2023.126807.
[35] Gubesch E, Abdussamie N, Penesis I, Chin C. Maximising the hydrodynamic performance of offshore oscillating water column wave energy converters. Appl Energy 2022;308. http://dx.doi.org/10.1016/j.apenergy.2021.118304.
[36] Shao X, Ringsberg JW, Yao H-D, Johnson E, Forsberg J, Zeinali S, Lindström J, Wiktorsson M. A comparison of approaches integrating power take-off systems into wave energy converters simulations. CRC Press; 2024, p. 351–8.
[37] Shao X, Ringsberg JW, Yao H-D, Gowda URSL, Khedkar HN, Todalshaug JH. Hydrodynamic interactions and enhanced energy harnessing amongst many WEC units in large-size wave parks. J Mar Sci Eng 2024;12(5). http://dx.doi.org/10.3390/jmse12050730.
[38] Quartier N, Vervaet T, Fernandez GV, Domínguez JM, Crespo AJC, Stratigaki V, Troch P. High-fidelity numerical modelling of a two-WEC array with accurate implementation of the PTO system and control strategy using DualSPHysics. Energy 2024;296. http://dx.doi.org/10.1016/j.energy.2024.130888.
[39] Shao X, Yao H-D, Ringsberg JW, Li Z, Johnson E. Performance analysis of two generations of heaving point absorber WECs in farms of hexagon-shaped array layouts. Ships Offshore Struct 2024;1–12. http://dx.doi.org/10.1080/17445302.2024.2317658.
[40] Palm J, Eskilsson C, Paredes GM, Bergdahl L. Coupled mooring analysis for floating wave energy converters using CFD: Formulation and validation. Int J Mar Energy 2016;16:83–99. http://dx.doi.org/10.1016/j.ijome.2016.05.003.
[41] Penalba M, Davidson J, Windt C, Ringwood JV. A high-fidelity wave-to-wire simulation platform for wave energy converters: Coupled numerical wave tank and power take-off models. Appl Energy 2018;226:655–69. http://dx.doi.org/10.1016/j.apenergy.2018.06.008.
[42] Yang Y, Bashir M, Michailides C, Li C, Wang J. Development and application of an aero-hydro-servo-elastic coupling framework for analysis of floating offshore wind turbines. Renew Energy 2020;161:606–25. http://dx.doi.org/10.1016/j.renene.2020.07.134.
[43] Cao FF, Yu MQ, Han M, Liu B, Wei ZW, Jiang J, Tian HY, Shi HD, Li YN. WECs microarray effect on the coupled dynamic response and power performance of a floating combined wind and wave energy system. Renew Energy 2023;219. http://dx.doi.org/10.1016/j.renene.2023.119476.
[44] Han M, Shi H, Cao F, Zhu K, Liu B, Yu M, Wei Z. Dynamic characteristics and parameter analysis of a floating hybrid wind-wave energy system based on a novel coupled numerical framework. Energy Convers Manage 2024;312. http://dx.doi.org/10.1016/j.enconman.2024.118558.
[45] Jin P, Zheng Z, Zhou Z, Zhou B, Wang L, Yang Y, Liu Y. Optimization and evaluation of a semi-submersible wind turbine and oscillating body wave energy converters hybrid system. Energy 2023;282. http://dx.doi.org/10.1016/j.energy.2023.128889.
[46] FMI. FMU tools. 2023, URL https://fmi-standard.org/tools/.
[47] Ansys Inc. Ansys twin builder. 2023, URL https://www.ansys.com/products/digital-twin/ansys-twin-builder.
[48] MathWorks, Inc. Simulink. 2023, URL https://www.mathworks.com/products/simulink.html Version R2023a.
[49] Yuan R, Fletcher T, Ahmedov A, Kalantzis N, Pezouvanis A, Dutta N, Watson A, Ebrahimi K. Modelling and co-simulation of hybrid vehicles: A thermal management perspective. Appl Therm Eng 2020;180. http://dx.doi.org/10.1016/j.applthermaleng.2020.115883.
[50] Sanfilippo F, Hatledal LI, Pettersen KY, Zhang H. A benchmarking framework for control methods of maritime cranes based on the functional mockup interface. IEEE J Ocean Eng 2018;43(2):468–83. http://dx.doi.org/10.1109/joe.2017.2691920.
[51] Gan J, Zhou Z, Yu A, Ellis D, Attwood R, Chen W. Co-simulation of multibody dynamics and discrete element method for hydraulic excavators. Powder Technol 2023;414. http://dx.doi.org/10.1016/j.powtec.2022.118001.
[52] ITEA4. Modelisar. 2024, URL https://itea4.org/project/modelisar.html.
[53] Clagms. The functional mock-up interface beginners' tutorial. 2023, URL https://github.com/modelica/fmi-beginners-tutorial-2023/blob/main/part3/into-cps_demo.pdf.
[54] Newman J. Marine hydrodynamics. The MIT Press; 2018.
[55] Faltinsen O. Sea loads on ships and offshore structures. vol. 1, Cambridge University Press; 1993.

[56] Aqwa theory manual. ANSYS Inc.; 2023, Version 2023 R1.
[57] Sheng W. Wave energy conversion and hydrodynamics modelling technologies: A review. Renew Sustain Energy Rev 2019;109:482–98. http://dx.doi.org/10.1016/j.rser.2019.04.030.
[58] Kramer MB, Andersen J, Thomas S, Bendixen FB, Bingham H, Read R, Holk N, Ransley E, Brown S, Yu Y-H, Tran TT, Davidson J, Horvath C, Janson C-E, Nielsen K, Eskilsson C. Highly accurate experimental heave decay tests with a floating sphere: A public benchmark dataset for model validation of fluid–structure interaction. Energies 2021;14(2). http://dx.doi.org/10.3390/en14020269.
[59] Shao X, Ringsberg JW, Yao H-D, Li Z, Johnson E, Fredriksson G. A comparison of two wave energy converters' power performance and mooring fatigue characteristics – one WEC vs many WECs in a wave park with interaction effects. J Ocean Eng Sci 2023;8(4):446–60. http://dx.doi.org/10.1016/j.joes.2023.07.007.
[60] Wang T, Zhu K, Cao F, Li D, Gong H, Li Y, Shi H. A coupling framework between OpenFAST and WEC-Sim. Part I: Validation and dynamic response analysis of IEA-15-MW-UMaine FOWT. Renew Energy 2024;225. http://dx.doi.org/10.1016/j.renene.2024.120249.
[61] Alves M. Numerical modelling of wave energy converters. Elsevier; 2016, p. 11–30. http://dx.doi.org/10.1016/b978-0-12-803210-7.00002-5, book section 2.